Endothelial Cell Structure Changes on Native Compared to Glycated Collagen in Response to Substrates of Different Stiffness

A Thesis

Submitted to the Faculty

of

Drexel University

by

Aniel Padrino

in partial fulfillment of the

requirements for the degree

of

Master of Science in Mechanical Engineering

JUNE 2012

Acknowledgements

I will be forever grateful to my advisor Dr. Alisa Clyne Morss Clyne, thanks to her patience and advice I was able to continue working even in those moments in which I felt I could not go anymore. These types of scientific investigations require a student or investigator with a lot of dedication and motivation, and in instances in which both of these qualities were not within me it was good to have someone like Dr. Clyne overseeing me because not only is she a great motivator but also a great role model.

I am grateful for the support and advice I received from my fellow lab mates Dannielle, Steve, Becky, Adam, Nisha, Justin, Miao and Krishna. They were always available to answer my questions no matter how simple or complicated they were. I would like to thank Becky for helping me with the Atomic Force Microscopy experiments. I would also like to take this opportunity to thank Anant Chopra and Dr. Kresh for the many discussions we had where I learned a great deal about cardiovascular cell mechanics. I would like to thank Anant for showing me what it takes to be a scientist through his work he served me as an inspiration and guide during my own investigations.

Most importantly I would like to dedicate this thesis to my family. To my parents who have always been next to me inspiring me and providing all of their unconditional support. Without them none of this would of have been possible.

Table of Contents

Acknowledgements iii

List of Tables vii

List of Figures viii

Abstract xii

1 Introduction 1

1.1 Cell mechanics: Response to substrates of different stiffness 1

1.2 Cell mechanics techniques: Traction force microscopy and atomic force microscopy 5

1.3 Endothelial cell mechanics: Effects of collagen glycation and substrate stiffness 7

2 Polyacrylamide Hydrogel Engineering and Protein Crosslinking 10

2.1 Introduction 10

2.2 Methods 10

2.2.1 Creating PA gels of different stiffness coated with collagen 10

2.2.2 Collagen labeling on PA substrates 13

2.2.3 Rheology 14

2.3 Results 15

2.3.1 PA gels 15

2.3.2 Protein conjugation verification 16

2.3.3 Rheology measurements 17

2.4 Discussion 17

2.5 Conclusions 18

3 Endothelial Cell Morphology and Adhesion 19

3.1 Introduction 19
3.2 Methods 20
3.2.1 Endothelial cell culture, collagen glycation and immunofluorescent microscopy 20
3.2.2 Endothelial cell morphology measurements 21
3.2.3 Endothelial cell focal adhesion number and size 22
3.2.4 Statistical Analysis 23
3.3 Results 24
3.3.1 Endothelial cell images 24
3.3.2 Quantitative analysis of cell morphology 31
3.3.3 Focal adhesion size and number 34
3.3.4 50:50 native and glycated collagen coated substrates 37
3.4 Discussion 40
3.5 Conclusion 42
4 Endothelial Cell Traction Forces 43
4.1 Introduction 43
4.2 Methods 44
4.2.1 PA gel micropatterning 44
4.2.2 Endothelial cell traction force measurement 46
4.2.3 Endothelial cell cytoskeleton stiffness 46
4.3 Results 47
4.3.1 Micropattern transfer to PA gel 47
4.3.2 Endothelial traction force microscopy 48

4.3.3 Endothelial cell stiffness 56

4.4 Discussion 57

4.5 Conclusion 60

5 Conclusion and Future Work 60

5.1 Future Work 61

List of References 63

List of Tables

Table 2.1 PA gel shear modulus as a function of acrylamide and bisacrylamide concentrations. 11

Table 3.1 Pearson product-moment correlation analysis for focal adhesion size and number vs. cell area for native and glycated-coated substrates. 37

List of Figures

Figure 2.1 PA gel polymerization schematic. (A): PA solution sandwiched between hydrophobic and hydrophilic coverslips. (B): Approximately 5 minutes after adding gel solution the top coverslip was removed. (C): Final PA gel is flat after removing top coverslip 12

Figure 2.2 Functionalization procedure for PA gels. (A): The surface is activated upon sulfo-SANPAH addition, which is catalyzed with UV light. (B): ECM protein is incubated with the PA hydrogel overnight. (B): Completed functionalization of ECM protein to PA hydrogel. 13

Figure 2.3 Photograph of cross-linked PA gel on 22 by 22 mm glass coverslip after removing hydrophobic top glass coverslip. The gel has a flat top surface and remains attached to the hydrophilic bottom glass coverslip. 15

Figure 2.4. Fluorescent labeling showed that collagen was conjugated to sulfo-SANPAH on PA gels. (A): fluorescent image showing a collagen layer (green) on the top surface of a PA gel. (B): phase contrast image of the PA gel surface. (C): fluorescent image showing no collagen in the middle of a PA gel. (D): phase contrast image of the middle of a PA gel. 16

Figure 2.5. Experimental shear modulus data obtained from rheological measurements compared to theoretical shear modulus obtained from literature..... 17

Figure 3.1 Actin gray scale image of a PAEC (A). Gray scale image after smoothing using GaussianBlur tool (B). Binary processed image after thresholding (C). Image C is used to obtain morphological measurement using ImageJ particle analyzing plugins. 21

Figure 3.2 Focal adhesion image processing from grayscale to binary. (A): unprocessed grayscale image of focal adhesion sites on a cell. (B): grayscale image after background noise is reduced. (C): grayscale after it has been sharpened using the Unsharpmask tool. (D): binary image after thresholding showing focal adhesion sites in black 23

Figure 3.3 On native collagen, PAEC show more actin fibers and focal adhesion formation as stiffness increases; this trend is not as apparent in cells on glycated collagen. Fluorescent images of PAEC seeded on: soft PA gels (G = 0.3 kPa), physiological stiffness PA gels (G = 5 kPa, 10 kPa), stiff PA gels (G = 18kPa, 30 kPa) and glass. Cells were labeled for F-actin (red), vinculin (green) and nuclei (blue). Scale bar = 20 μm. ... 24

Figure 3.4 Cells on both native (A) and glycated (B) collagen coated 0.3 kPa gels showed little spreading or actin fiber formation. Cells were labeled for F-actin (red), vinculin (green) and nuclei (blue). Scale bar = 20 μm. 26

Figure 3.5 On 5 kPa gels, cells on native collagen (A) had larger spread area and showed more developed F-actin fibers than cells on glycated collagen (B). Cells were labeled for F-actin (red), vinculin (green) and nuclei (blue). Scale bar = 20 μm. 27

Figure 3.6 On 10 kPa gels, cells on native collagen (A) had larger spread area and showed more developed F-actin fibers than cells on glycated collagen (B). Cells were labeled for F-actin (red), vinculin (green) and nuclei (blue). Scale bar = 20 μm. 27

Figure 3.7 On 18 kPa gels, cells on native collagen (A) showed more developed F-actin stress fibers and focal adhesion formation compared to cells on glycated collagen (B). Cells were labeled for F-actin (red), vinculin (green) and nuclei (blue). Scale bar = 20 μm. 28

Figure 3.8 On 30 kPa gels, cells on native collagen (A) showed more developed F-actin stress fibers and focal adhesion formation compared to cells on glycated collagen (B). Cells were labeled for F-actin (red), vinculin (green) and nuclei (blue). Scale bar = 20 μm. 29

Figure 3.9 Cell on native (A) and glycated (B) collagen coated glass showed little difference in morphology, F-actin, and focal adhesion organization. Cells were labeled for F-actin (red), vinculin (green) and nuclei (blue). Scale bar = 20 μm..... 30

Figure 3.10 Cell area (A) and perimeter (B) increased with substrate stiffness on both native and glycated collagen coated substrates ($p < 0.01$ by ANOVA). However, at each stiffness level, cells on native collagen showed higher area and perimeter. (**$p < 0.01$ compared to native of same stiffness by Students t-test). Error bars indicated standard deviation..... 31

Figure 3.11. Curve fits of area (A) and perimeter (B) vs. substrate shear modulus for cells on native collagen. One-phase exponential fit. Area: $R^2 = 0.968$. Perimeter: $R^2 = 0.9901$. 32

Figure 3.12. Curve fit of area (A) and perimeter (B) vs. substrate shear modulus for cells on glycated collagen. One-phase exponential curve fit. Area: $R^2 = 0.7601$. Perimeter: $R^2 = 0.8589$. 33

Figure 3.13. Cell shape indices for PAEC on PA gels and glass coated with native and glycated collagen did not exhibit consistent trends. (A) Aspect ratio, (B) circularity. (**$p < 0.01$ compared to native of same stiffness by Students t-test). Error bars indicated standard deviation. 34

Figure 3.14 Focal adhesion size (A) did not change with gel stiffness but did increase on glass, and focal adhesion number (B) increased with stiffness on both native and glycated collagen coated substrates ($p < 0.01$ by ANOVA). Focal adhesion size and number were consistently lower in cells on glycated collagen compared to native collagen (*$p < 0.05$, **$p < 0.01$ compared to native of same stiffness by Students t-test)..... 36

Figure 3.15. Focal adhesion size and number compared to average cell area on native (A) and glycated (B) substrates. Only focal adhesion number in cells on native collagen increased linearly with cell area ($R^2 = 0.998$). 37

Figure 3.16 Fluorescent images of PAEC seeded on 50:50 native:glycated collagen coated gels. Cell area as well as actin fiber and focal adhesion formation at the individual stiffnesses looked similar to that of cells on native collagen. Cells were labeled for F-actin (red), vinculin (green) and nuclei (blue). Scale bar = 20 μm 38

Figure 3.17 Cells on 50:50 native and glycated collagen substrates were similar in morphology and focal adhesion formation to cells on native collagen substrates. A: Cell area. B: Cell aspect ratio. C: Focal adhesion number and D: Focal adhesion size. (*$p < 0.05$ and **$p < 0.01$ compared to 50:50 native:glycated collagen data by Students t-test) 39

Figure 4.1 Process of making patterned gels using a PDMS stamp. (A): fluorescently labeled BSA was adsorbed onto a plasma-treated stamp. (B): BSA was stamped onto a glass coverslip. (C): the glass coverslip was placed on a PA gel pre-polymer. (D): the top coverslip was removed and the pattern was transferred to the gel. (E): Photograph of glass coverslip stamping. 45

Figure 4.2 Tetramethylrhodamine-labeled bovine serum albumin (TMR-BSA) micropattern transferred onto PA gel using a PDMS stamp. 48

Figure 4.3 Traction force measurement of PAEC on 1.8 kPa gel coated with native collagen. (A): Fluorescent image of the null pattern. (B): Fluorescent image of the cell stressed patterned dot grid. (C): Cell traction heat map with stress magnitude and direction. 49

Figure 4.4 Traction force measurement of PAEC on 5 kPa gel coated with native collagen. (A): Fluorescent image of the null pattern. (B): Fluorescent image of the cell stressed patterned dot grid. (C): Cell traction heat map with stress magnitude and direction. 50

Figure 4.5 Traction force measurement of PAEC on 10 kPa gel coated with native collagen. (A): Fluorescent image of the null pattern. (B): Fluorescent image of the cell stressed patterned dot grid. (C): Cell traction heat map with stress magnitude and direction. 51

Figure 4.6 Traction force measurement of PAEC on 5 kPa gel coated with glycated collagen. (A): Fluorescent image of the null pattern. (B): Fluorescent image of the cell stressed patterned dot grid. (C): Cell traction heat map with stress magnitude and direction. 53

Figure 4.7 Traction force measurement of PAEC on 10 kPa gel coated with glycated collagen. (A): Fluorescent image of the null pattern. (B): Fluorescent image of the cell stressed patterned dot grid. (C): Cell traction heat map with stress magnitude and direction. 54

Figure 4.8 Average cell traction (A) and cell area (B) for cells seeded on native and glycated collagen coated gels of different stiffness computed using the LIBTRC 2.4 software. 55

Figure 4.9 Endothelial cell shear modulus of elasticity increased on glass as compared to PA gels. (*p < 0.05 compared to glass on native collagen by Students t-test). Error bars indicate standard deviation. Number of samples was between 6 and 16. 57

Abstract
Endothelial Cell Structure Changes on Native Compared to Glycated Collagen in Response to Substrates of Different Stiffness
Aniel Padrino
Alisa Morss Clyne, PhD

Many diseases alter both the stiffness and composition of the extracellular matrix. Of particular interest to us is that diabetic hyperglycemia leads to collagen glycation, which both stiffens the extracellular matrix and alters cell-matrix interactions. Endothelial cells attach to matrix proteins via integrins clustered at focal adhesions. Cells transmit forces to integrins and extracellular matrix through the cytoskeleton, which deform substrates that are within a physiological stiffness range but not rigid substrates. As a consequence, cell morphology and function depend on substrate stiffness.

We hypothesized that collagen glycation affects endothelial response to substrates of different stiffness by altering cell-matrix interactions. To investigate this hypothesis, we seeded porcine aortic endothelial cells for 24 hours on native and glycated collagen-coated polyacrylamide gels with varying shear moduli (0.3 kPa – 30 kPa), as well as coated glass cover slips as a rigid control. Cells were labeled with rhodamine phalloidin and a vinculin antibody to visualize the actin cytoskeleton and focal adhesions, respectively. Cell morphology, including area, aspect ratio, and focal adhesion size and number were measured.

Cell area and focal adhesion number and size increased with substrate stiffness on both native and glycated collagen. However, cell area on native collagen increased 625% as gel stiffness increased from 0.3 kPa to 30 kPa, while cell area on glycated collagen coated gels increased only 139%. In contrast, cells on gels coated with glycated collagen

increased focal adhesion number by 32% and size by nearly 439%, whereas cells on native collagen increased focal adhesion number by over 100% and size by 1140% as gel stiffness increased from 5 kPa to 30 kPa. No focal adhesion sites were observed on cells seeded on 0.3 kPa gels coated with either native or glycated collagen. Cells on glass had the largest cell area, with no difference in area or focal adhesion size and number between native and glycated collagen coatings. Preliminary results from cell traction force studies revealed that on a 5 kPa gel, the average cell traction stress was 78% higher on native compared to glycated collagen and on the 10 kPa gel, the average cell traction stress was 33% higher on native compared to glycated collagen.

These data suggest that endothelial cell response to substrate stiffness is altered in disease conditions as cells are unable to properly spread, form focal adhesions and exert traction forces on glycated compared to native collagen coated substrates. These findings shed new light on how endothelial cell mechanotransduction can be impaired by disease conditions.

1 Introduction

1.1 Cell mechanics: Response to substrates of different stiffness

Cells, like many other engineered structures, need a foundation capable of providing mechanical support. In fact, most cell types require substrate adhesion to survive, proliferate, migrate, and assemble into a functional tissue. These cell functions are all performed *in vivo* on extracellular matrix (ECM). The ECM is a mesh composed of different proteins such as fibronectin, vitronectin and collagen that provides both mechanical support for surrounding cells and a variety of biochemical and biophysical signals that influence cellular behavior. .

The ECM can be defined in terms of its mechanical properties, such as the modulus of elasticity (*E)* or "stiffness" as it is most commonly known. Biological tissue stiffness varies among tissues: brain (E ~ 0.1-1 kPa) is softer than muscle (E ~ 8-17kPa) which in turn is softer than precalcified bone (E ~ 25-40 kPa) [1]. Anchorage-dependent cells sense ECM stiffness and respond through a variety of cellular processes. A thorough understanding of the effect of ECM mechanical properties on cell physiology and the mechanisms by which ECM stiffness has such a marked effect on cell response are of great importance in understanding both healthy tissue function and the origin and progression of diseases such as cancer and atherosclerosis [2].

The backbone of the cell is called the cytoskeleton. The cytoskeleton controls various cell functions. It determines cell mechanical properties by providing mechanical strength and integrity. It also serves as a highway for biochemical signals within the cell as well as an

anchor for the many different subunits inside the cell. The cell cytoskeleton is composed of three types of filaments called F-actin, intermediate filaments and microtubules. Actin is particularly important for stability, mobility and force generation. Cross-linked F-actin microfilaments dynamically remodel in response to mechanical forces and exert tensile forces throughout the cell and to the ECM through actin bundles called stress fibers [3].

Cells use 24 different types of integrins as ligands to ECM proteins such as collagen. Integrins are transmembrane heterodimers formed of α and β subunits. Different integrins are used by cells to attach to different ECM proteins. For example, $\alpha_2\beta_1$ integrin is primarily used to attach to collagen Type I whereas $\alpha_5\beta_1$ integrin is primarily used to attach to fibronectin and $\alpha_V\beta_3$ integrin is primarily used to attach to vitronectin. When cells are subjected to mechanical forces, integrins assemble into focal complexes that can mature into larger focal adhesions. These focal adhesions can contain 50 different proteins. Some proteins, such as vinculin and talin, provide sites for anchoring actin stress fibers, whereas others, such as focal adhesion kinase, provide biochemical signaling [2].

When external forces are applied, cells exert traction forces on the substrate to which they are attached via focal adhesions. Focal complex organization and maturation into focal adhesions enhances force transmission and also further increases adhesion maturation. Conversely, focal adhesion formation requires tension generated by actin fibers within the cell. The substrate resists these cell-generated forces if it is sufficiently stiff to prevent deformation [4]. Cells generate forces at ECM attachment sites, which can deform softer materials but not rigid surfaces. As a consequence, cell morphology and function depend strongly on substrate stiffness independent of chemical signaling [5].

Studying cells on substrates of different stiffness is physiologically relevant because cells change function with substrate stiffness and ECM stiffness varies among tissues and in disease states. To better understand how cells respond to the ECM, it is important to study single cells attached to substrates of different stiffness. It is expected that cells should vary their morphology and adhesion response as well as the traction forces applied to the ECM.

Cell mechanical response to substrates of different stiffness has been extensively studied. Materials such as polydimethylsiloxane (PDMS), polyethylene glycol (PEG), and hyaluronic acid (HA) are some of the synthetic and natural substrates with tunable elasticity that have been previously used to study cell response to substrate stiffness [1]. More recently, polyacrylamide (PA) has been used because it has several important features that set it apart from the other materials. PA gels allow systematic and reproducible control of substrate flexibility by varying the relative acrylamide and bis-acrylamide concentrations. PA gels have nearly ideal elastic behavior on both macro- and microscopic scales. These gels also have superb optical quality that permits high resolution immunofluorescent microscopy. Since PA gels do not interact with the cell surface, specific ECM molecules can be attached to the gels to control the cell adhesion ligand [6].

Previous studies examined the relationship between cell morphology and PA substrates of different stiffness. Cell morphology was measured for fibroblasts, endothelial cells, and neutrophils cultured on PA substrates with stiffnesses ranging from 2 to 55,000 Pa. The PA gels were coated with fibronectin or collagen as the adhesive ligand. When grown in sparse culture with no cell-cell contacts for a day, fibroblasts and endothelial

cells show an abrupt change in spread area that became noticeable at around 3,000 Pa. Fibroblast shape ranged from rounded cells on 180 Pa gels to large spread cells on gels stiffer than 16,000 Pa for both fibronectin and collagen coatings. Fibroblasts grown on gels softer than 1,600 Pa had no detectable stress fibers, whereas fibroblasts on gels stiffer than 3,600 Pa showed extensive stress fiber formation. Aortic endothelial cells showed a similar cell shape dependence on substrate stiffness. After one day of culture, cell spread area increased with substrate stiffness. However, cell spreading on collagen was lower for endothelial cells and fibroblasts compared to fibronectin coated gels. Finally, in contrast to both fibroblasts and endothelial cells, neutrophils kept a constant spread area over different stiffness range [5].

A related study was performed on bovine aortic endothelial cells seeded on PA substrates of different stiffness (1 to 10 kPa) coated with 100 μg/mL collagen. Endothelial cell morphology changed from spindle shaped on soft gels to more isotropic spreading with increased stiffness. Measurements of endothelial cell area revealed an increase from 1100 μm^2 to 2500 μm^2 as substrate stiffness increased from 1 to 10 kPa [7]. Another study using human aortic smooth muscle cells seeded on PA gels of different stiffness coated with fibronectin similarly showed that cell spread area increased with substrate stiffness [8].

1.2 Cell mechanics techniques: Traction force microscopy and atomic force microscopy

Cells respond to substrate stiffness by exerting contractile or traction forces on the substrate. Traction forces are relevant because they can predict cell preferred migration direction [9]. Traction forces are most commonly measured by traction force microscopy (TFM). In this method, the cell-induced substrate deformation is analyzed through the movement of fluorescent beads embedded in the gel. The bead displacement, x, is measured optically before and after the cell applies the traction force. The corresponding force (F) is calculated using the experimentally determined substrate elastic stiffness (k) which can be expressed in terms of the substrate's stiffness (E) [10]. While the specific equations depend on the traction force microscopy method, the general approach uses the linear relationship between displacement and force given by:

$$\boldsymbol{F} = -k\boldsymbol{x} \tag{1.1}$$

The methods used to determine substrate deformation have advanced over time. Initially, deformation was determined by identifying corresponding markers in the micrographs with and without applied traction forces. These markers would then be used to construct a force vector map. This method now has been replaced with automated computer algorithms like the one created by Micah Dembo and Yu-Li Wang. This method first captures bead marker displacement using a correlation-based optical flow algorithm by setting a grid on the image with no cell traction with the objective of tracking displacement of the grid markers. Once the displacement field is obtained the traction

vector field is constructed using the elastic solid Boussinesq solution [11] in which equation 1.1 becomes

$$\boldsymbol{d}_i = \sum_{j=1}^{m} \boldsymbol{G}(\boldsymbol{r}_{ij})\boldsymbol{F}_j \tag{1.2}$$

where $\boldsymbol{d}_i$ is the marker's displacement vector field due to various force vectors $\boldsymbol{F}_j$. Both vectors contain x and y components, and $\boldsymbol{r}_{ij} = \boldsymbol{x}_i - \boldsymbol{x}_j$ is the distance vector. $\boldsymbol{G}(\boldsymbol{r})$ is defined by the Boussinesq theory as

$$\boldsymbol{G}(\boldsymbol{r}) = \frac{1+\upsilon}{\pi E r^3}\begin{bmatrix}(1-\upsilon)r^2 + \upsilon r_x^2 & \upsilon r_x r_y \\ \upsilon r_x r_y & (1-\upsilon)r^2 + \upsilon r_y^2\end{bmatrix} \tag{1.3}$$

where $r = \sqrt{\boldsymbol{r}\cdot\boldsymbol{r}}$, E is the substrate's Young modulus and υ is Poisson's ratio [12].

Dembo's method makes assumptions such as the thickness of the elastic substrate is effectively infinite compared to the maximum marker displacement and as a result an accurate approximation for equation 1.3 can be derived [11]. The traction vector field is obtained from equation 1.2 by a recovery process in which the *m* force vectors are obtained given the *n* amount of displacement vectors. Dembo proposed the traction force recovery problem as a regularized parameter estimation problem in which the regularization factor λ varies from 0 to 1 [12].

Recent studies showed that cell traction forces (CTF) vary on substrates of different stiffness. The average myocyte contractile forces increased with PA substrate stiffness [13]. Human dermal fibroblasts seeded on fibronectin coated substrates of different stiffness showed that average cell-induced traction force increased with substrate stiffness [14]. Similarly, bovine aortic endothelial cells seeded on PA substrates of different

stiffness coated with collagen demonstrated traction forces that increased significantly from 200 Pa to 400 Pa as stiffness increased from 1 to 10 kPa [7].

Cells also change cytoskeletal assembly in response to substrate stiffness, which can affect the stiffness of the cell itself [15]. Cell stiffness can be measured by many techniques, including atomic force microscopy (AFM). In AFM, a small force is applied to the cell surface using a flexible silicon cantilever. Cantilever deflection is measured via a laser reflected off the top of the cantilever. Laser light intensity is then converted to voltage and finally to displacement. Cantilever tip deflection is then converted to force F using equation 1.1, where cantilever stiffness k is calibrated independently via deflection against a rigid surface such as glass [10].

Previous studies of cell stiffness on PA substrates of different stiffness revealed the relationship between these two mechanical factors. Fibroblasts increased in stiffness from 6 to 8 kPa when seeded on 20 kPa gels and glass; this change also correlated with more organized stress fibers observed on glass [15]. Myocytes seeded on PA substrates of different stiffness revealed that cell stiffness increased from 4 to 8 kPa as substrate stiffness increased from 0.3 to 30 kPa [13]. A similar trend was also observed in human mesenchymal stem cells seeded on PA gels of different stiffness [16].

1.3 Endothelial cell mechanics: Effects of collagen glycation and substrate stiffness

Diabetic hyperglycemia, or elevated blood glucose, is common to both insulin deficient type I and the more prevalent insulin resistant type II diabetes [17]. Although cardiovascular disease has been a focus of intensive research in patients with diabetes, for

decades, it is only in recent years that the role of hyperglycemia as a risk factor for cardiovascular disease has been clarified. Before the 1990s, hyperglycemia was not believed to contribute to cardiovascular disease in type II diabetes. However, more recent studies indicate that hyperglycemia is an important risk factor for cardiovascular disease [18]. The San Antonio Heart Study demonstrated that hyperglycemia is a risk factor not only in Caucasians, but also in other ethnic groups [19] while the Wisconsin Epidemiologic Study of Diabetic Retinopathy showed the importance of glycemic control for micro- and macrovascular complications [20].

Chronic hyperglycemia leads to endothelial cell dysfunction both *in vivo* and *in vitro*, and loss of endothelial function has been implicated in diabetic vascular disease development. Endothelial cells actively regulate vascular tone and vascular reactivity in physiological and pathological conditions by responding to mechanical factors such as shear stress and cyclic strain from the flowing blood [21, 22].

Diabetic hyperglycemia leads to ECM protein non-enzymatic glycosylation (or glycation) as a function of time and glucose concentration [23]. Glucose glycates both collagen and fibronectin via the Maillard reaction, in which glucose reacts with amino protein groups to eventually form irreversible advanced glycation end products (AGEs) [24]. AGE formation on ECM proteins interferes not only with matrix-matrix interactions but also with matrix-cell interactions. Glycation affects ECM protein cell-binding domains, which inhibits cell adhesion and spreading on the ECM [25].

While many studies demonstrated endothelial cell biochemical dysfunction on glycated substrates, limited studies have shown endothelial cell mechanical dysfunction when cells

are cultured on glycated collagen substrates. Endothelial cells on native collagen aligned and formed actin stress fibers perpendicular to the stretch direction after 6 hours of cyclic strain, while cells on glycated collagen did not align even after 12 hours of cyclic strain [26]. Similarly, endothelial cells grown on native collagen elongated and aligned in the flow direction due to fluid shear stress, whereas cells on glycated collagen did not align [27]. In these studies, the authors propose that there may be a change in the mechanism of cell binding to glycated collagen that inhibits the cyclic strain and shear stress responses.

These studies show that endothelial cells alter their mechanical function in response to collagen glycation. However, both studies were performed on endothelial cell monolayers. Little is known about how single endothelial cells react to substrates of different stiffness that are coated with native vs. glycated collagen. I hypothesized that glycated collagen would alter endothelial cell morphological response to substrates of different stiffness. To investigate this hypothesis, I created PA gels of different stiffness that were coated with native or glycated collagen (Chapter 2). I then measured changes in endothelial cell morphology on these substrates and compared the effects of native and glycated collagen (Chapter 3). Finally, I determined cell traction forces on substrates of different stiffness coated with native and glycated collagen (Chapter 4). This thesis describes these results, which clearly demonstrate that collagen glycation affects cell response to substrate stiffness.

2 Polyacrylamide Hydrogel Engineering and Protein Crosslinking

2.1 Introduction

Polyacrylamide (PA) hydrogels are one of the many engineering materials used to control substrate stiffness for *in vitro* cell culture experiments. Polyacrylamide substrates have several important features that set them apart from the other materials used in cell studies. PA gels are of superb optical quality. They can be constructed of minimal thickness, which allows high magnification fluorescent imaging of intracellular components. PA gels also show nearly ideal elastic mechanical behavior at both macro- and microscopic scales. Most importantly, PA gel stiffness can be reproducibly controlled. PA gels of different mechanical stiffness can be engineered by varying the relative acrylamide and bis-acrylamide concentrations. These hydrogels also do not readily bind proteins, which means that a specific protein can be covalently bound to the PA gel surface to control the mechanism of cell-substrate interactions [6].

In this chapter, I explain the engineering of collagen coated PA gels of varying stiffness.

2.2 Methods

2.2.1 Creating PA gels of different stiffness coated with collagen

PA gels of the desired stiffness were made by mixing varied acrylamide and bisacrylamide (Bio-Rad) concentrations with 10 mM HEPES (Sigma) as previously described [6]. Table 2.1 displays acrylamide and bisacrylamide concentrations used to

produce the desired shear modulus of elasticity *G'* as obtained from literature [5]. The shear modulus for each gel formulation was verified using rheological measurements (described below).

Table 2.1 PA gel shear modulus as a function of acrylamide and bisacrylamide concentrations.

Shear Modulus ('G), [kPa]	% Acrylamide	% Bis-acrylamide	Final volume [µL]	40% Acrylamide [µL]	2% Bis-acrylamide [µL]	10 mM HEPES [µL]
0.3	3	0.2	3000	225	300	2475
5	7.5	0.2	3000	562.5	300	2137.5
10	7.5	0.35	3000	562.5	525	1912.5
18	12	0.18	3000	900	270	1830
30	12	0.3	3000	562.5	450	1650

Acrylamide solutions were then cross-linked into a polymer on top of coverslips. 1.5 µl tetramethylethlylenediamine (Fisher) and 5 µl 10% ammonium persulfate (Fisher) were added to 10 mM HEPES for a total volume of 500 µl. A 0.4 mm thick polymer gel was achieved by depositing a 215 µl droplet on a 22 x 22 mm glass hydrophilic coverslip pretreated with 3-aminopropyltrimethoxysilane (Sigma) and 0.5% gluteraldehyde (Sigma). A second 22 x 22 mm hydrophobic coverslip (Fisher) treated with Surfasil (Thermo Scientific) was placed on top of the PA solution at room temperature. After approximately five minutes, the gel polymerized and the top coverslip was then removed as illustrated in Figure 2.1. The gel was then rinsed 3+ times for 5 minutes with 50 mM HEPES [1].

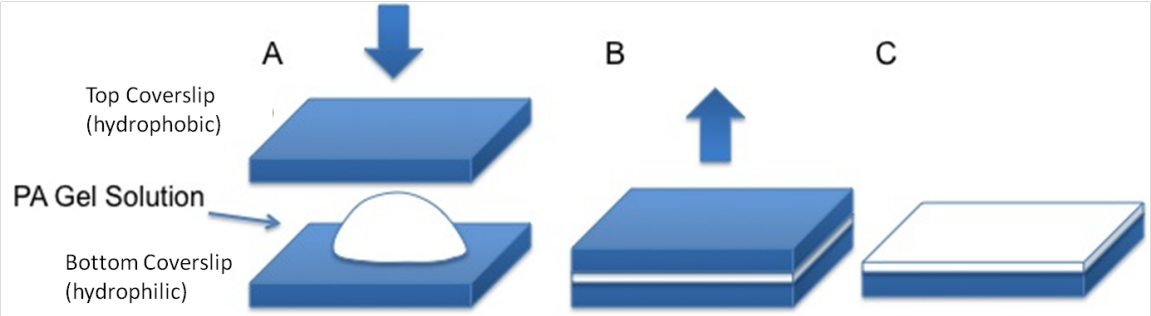

Figure 2.1 PA gel polymerization schematic. (A): PA solution sandwiched between hydrophobic and hydrophilic coverslips. (B): Approximately 5 minutes after adding gel solution the top coverslip was removed. (C): Final PA gel is flat after removing top coverslip

Since PA gels do not readily adsorb proteins or allow cell attachment, a collagen coating was covalently bound to the gel. Sulfo-SANPAH , a heterobifunctional protein cross-linker, was used to covalently bind native and glycated collagen to the PA substrates as previously described [1]. 200 µl of 0.2 mg/ml sulfo-SANPAH solution was added to the gel surface, after which gels were placed 3 inches below a UV light (365 nm) and irradiated for 7 minutes or until the solution turned dark. This process was repeated a second time to enhance protein binding. After the last treatment, 500 µl native or glycated collagen type I (100 µg/ml) was added to the gel and incubated overnight at 4°C. Gels were then thoroughly washed three times with phosphate buffered saline (PBS) for 5 minutes each. The process is illustrated in Figure 2.2.

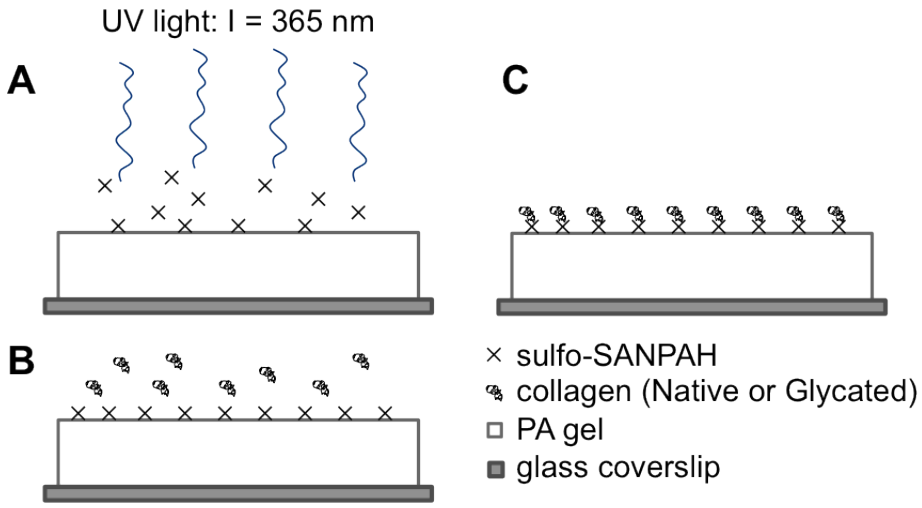

Figure 2.2 Functionalization procedure for PA gels. (A): The surface is activated upon sulfo-SANPAH addition, which is catalyzed with UV light. (B): ECM protein is incubated with the PA hydrogel overnight. (B): Completed functionalization of ECM protein to PA hydrogel.

For comparison, native and glycated collagen were also coated on 22 x 22 mm glass coverslips. Coverslips were washed with 70% ethanol (Fisher), exposed to UV light for one hour, treated with 0.5% gluteraldehyde for 30 minutes, and then washed with 50 mM HEPES. The treated glass substrates were then completely covered with native or glycated collagen type I (100 μg/ml) overnight at 4°C to allow protein binding.

2.2.2 Collagen labeling on PA substrates

To ensure uniform collagen coating on PA gels, collagen-coated PA gels were labeled by immunofluorescent microscopy. Briefly, collagen-coated gels were incubated with 1% bovine serum albumin (BSA) for 30 minutes at room temperature to block non-specific binding. After removing BSA solution, the gels were incubated with a monoclonal anti-type I collagen primary antibody (1:200, Sigma) for 2 hours at 37°C and 5% CO_2. Gels were washed 3 times for 5 minutes in PBS. Finally the gels were incubated with a

secondary antibody (1:200, AF 488, Invitrogen) for 1 hour at 37°C and 5% CO_2. Gels were washed 3 times with PBS for 5 minutes each. The top surface of the gel was imaged by fluorescent microscopy to ensure adequate collagen surface distribution. The gel center was also imaged to verify that collagen only attached to the surface and not inside the gel.

2.2.3 Rheology

Rheology measurements were performed on PA gels to verify expected shear modulus values. PA gel viscoelastic properties were quantified by measuring the dynamic shear moduli of a 500 μL gel between two 25-mm stainless steel parallel plates (sample thickness ~1 mm) using an RFS II fluids spectrometer (Bohlin Rheometer). The shear storage modulus *G'*, corresponding to the elastic resistance of the gels, was determined from the shear stress in phase with an oscillatory (1 rad/s) shear strain of 2% maximal amplitude as previously described [5].

2.3 Results

2.3.1 PA gels

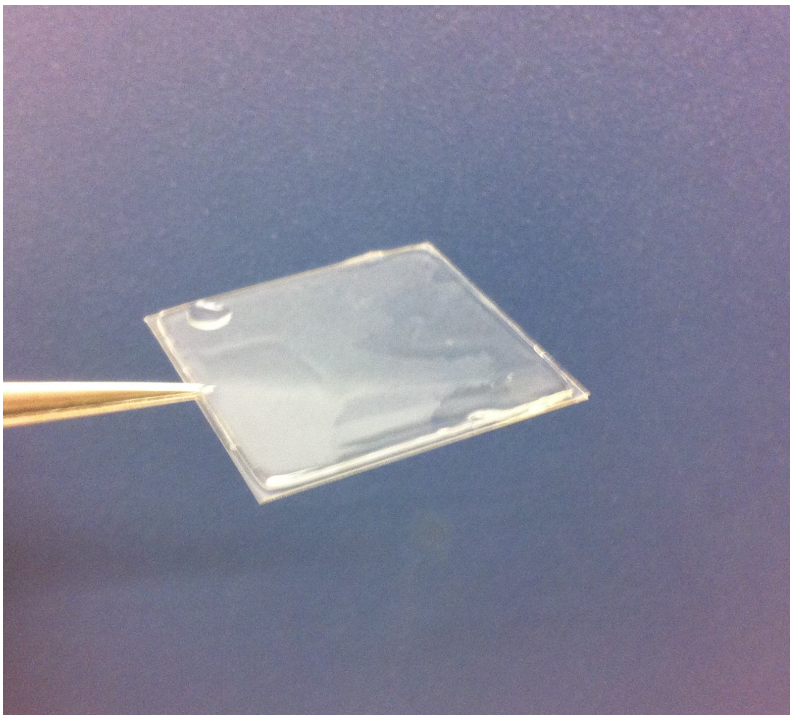

Figure 2.3 Photograph of cross-linked PA gel on 22 by 22 mm glass coverslip after removing hydrophobic top glass coverslip. The gel has a flat top surface and remains attached to the hydrophilic bottom glass coverslip.

Figure 2.3 shows a polymerized gel on a glass coverslip. The gel top surface remains flat, which is critical for effective imaging. The gel remains attached to the bottom coverslip due to the glass's hydrophilic properties.

2.3.2 Protein conjugation verification

Collagen conjugation via sulfo-SANPAH was verified using fluorescent microscopy. Figure 2.4 shows an evenly distributed collagen layer (green), demonstrating that collagen was successfully conjugated to the PA gel surface.

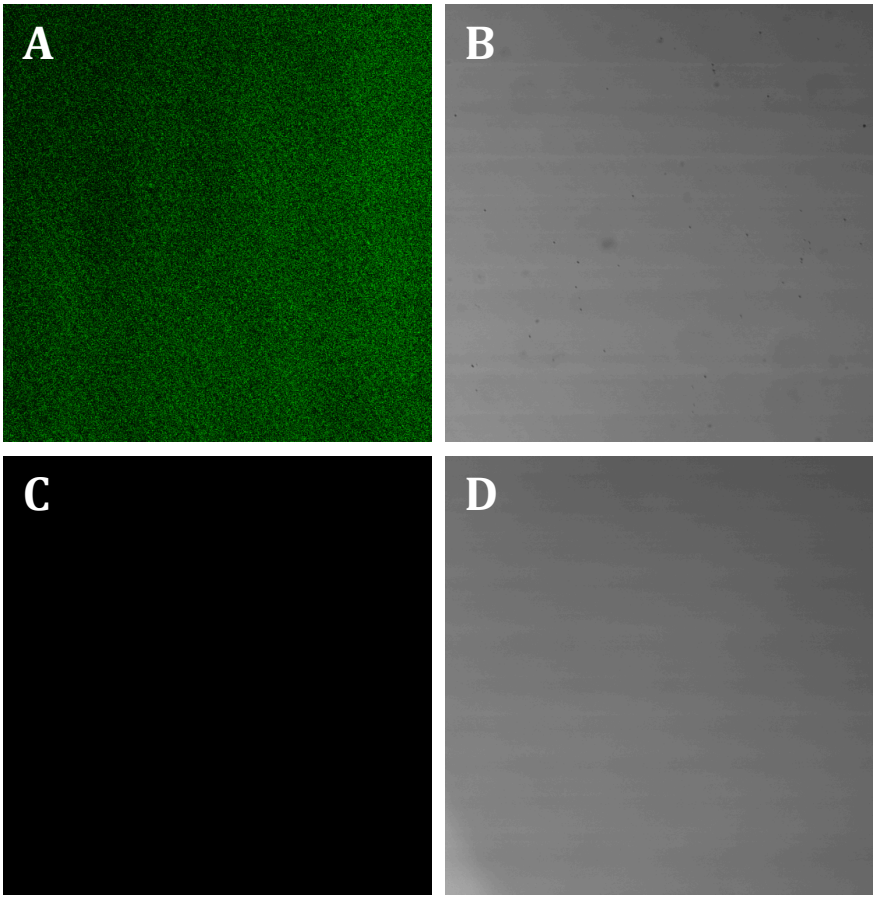

Figure 2.4. Fluorescent labeling showed that collagen was conjugated to sulfo-SANPAH on PA gels. (A): fluorescent image showing a collagen layer (green) on the top surface of a PA gel. (B): phase contrast image of the PA gel surface. (C): fluorescent image showing no collagen in the middle of a PA gel. (D): phase contrast image of the middle of a PA gel.

2.3.3 Rheology measurements

Rheological measurements were taken for each of the PA solutions to verify the published acrylamide and bisacrylamide concentrations required to achieve gels of a given stiffness. The percent difference between theoretical and experimental shear modulus was less than 6% for all gels tested except for the 300 Pa gel (Figure 2.5). The 300 Pa gel had an experimental shear modulus of 190 Pa, accounting for a 37% percent deviation from the theoretical value.

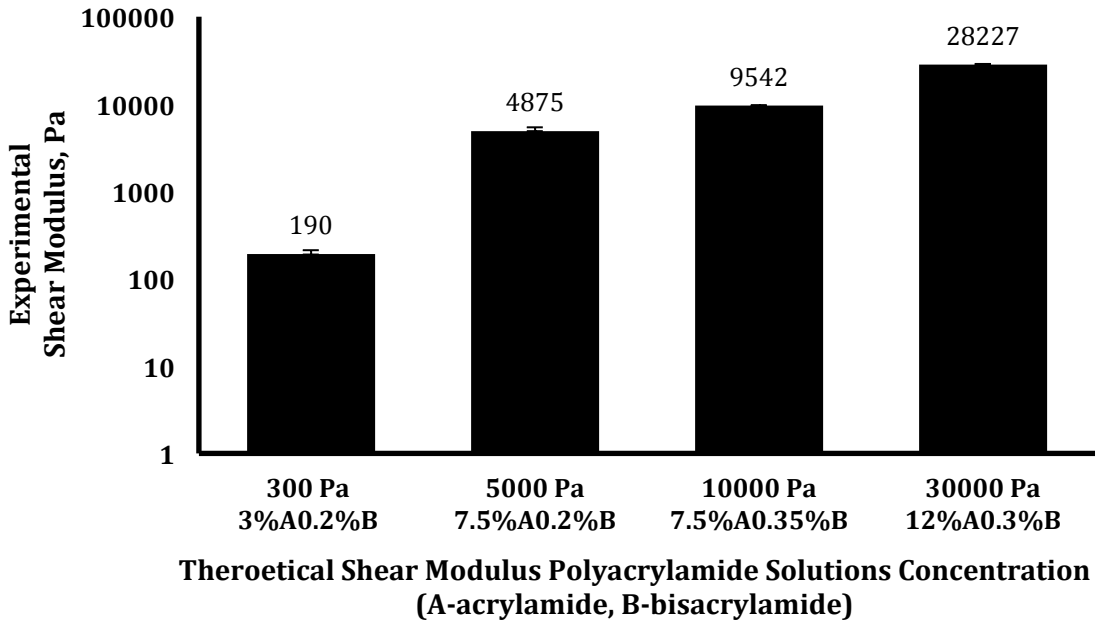

Figure 2.5. Experimental shear modulus data obtained from rheological measurements compared to theoretical shear modulus obtained from literature.

2.4 Discussion

In this chapter, I demonstrated that PA gels could be made of different stiffnesses, and that these gels could be coated with native and glycated collagen. Validation of the

theoretical shear modulus of elasticity by rheology showed that measured results were generally within 6% percent of the theoretical shear modulus. The 37% difference between experimental and theoretical results for the 300 Pa gel is likely due to experimental error either in mixing the acrylamide and bis-acrylamide or when performing measurements with the rheometer. Since the experimental measurements were close to the theoretical measurements, I subsequently refer to gels by their theoretical shear modulus in later chapters.

2.5 Conclusions

In this chapter, I demonstrated how to successfully manufacture PA gels of different stiffness coated with native and glycated collagen. These gels were then used to determine endothelial cell morphological response to substrates of different stiffness, and how that response depended on the native or glycated collagen coating (Chapter 3). The gels were also used to measure cell traction forces (Chapter 4).

3 Endothelial Cell Morphology and Adhesion

3.1 Introduction

The ECM alters cytoskeletal mechanics and changes cell shape by transmitting mechanical stress across integrins [28]. Previous studies have shown how cells spread and grow on rigid ECM, but they retract, round and differentiate on malleable foundations [29]. This same effect is observed for varied cell types and matrix proteins (e.g., fibronectin, collagen). However, endothelial cells have been shown to be dysfunctional when they interact with glycated collagen. Specifically relevant to my research, endothelial cells do not spread properly on glycated collagen substrates [25]. I therefore hypothesized that glycated collagen would alter endothelial cell morphological and cytoskeletal response to substrates of different stiffness.

Endothelial cells were sparsely seeded on PA gels of increasing stiffness that were coated with either native or glycated collagen, as described in Chapter 2. In this chapter, I present my analysis of endothelial cell morphology by measuring spread area and aspect ratio in actin-labeled cells. I further present changes in focal adhesions on the different substrates by measuring focal adhesion size and number via vinculin labeling. These results show how cellular mechanotransduction of substrate stiffness is changed by biochemical interactions between cells and matrix proteins.

3.2 Methods

3.2.1 Endothelial cell culture, collagen glycation and immunofluorescent microscopy

Porcine aortic endothelial cells (PAEC, passages 5 - 8) were cultured in Dulbecco's Modified Eagle Medium (DMEM, Mediatech) supplemented with 5% fetal bovine serum (FBS; Hyclone), 1% glutamine and 1% penicillin-streptomycin (Gibco). Cells were maintained at 37°C and 5% CO_2, with a medium change every two days. Collagen was glycated by incubating 100 μg/ml collagen type I (Sigma) with 500 mM D-glucose-6-phosphate (Sigma) in phosphate buffered saline (PBS) at 37°C for 4 weeks. Glycation was validated by collagen autofluorescence and Western blot [26]. Cells were seeded at 2,500 cells/cm^2 on native or glycated collagen coated PA gels and glass coverslips, placed in 6 well plates, and allowed to attach for 24 hours. Cells were then fixed with 4% paraformaldehyde for 15 minutes, permeabilized with 0.1% Triton X-100 for 5 minutes, and blocked with 1% bovine serum albumin (BSA) for 30 minutes at room temperature.

PAEC morphology was assessed by labeling actin filaments and nuclei with rhodamine phalloidin (1:60, Invitrogen) and Hoechst (1:2000, Invitrogen), respectively, for 30 minutes at 37°C. Focal adhesions were labeled with a mouse anti-human monoclonal vinculin antibody (1:100, Sigma) and a goat anti-mouse Alexafluor 488 secondary antibody (1:100, Invitrogen) at 37°C for an hour. Samples were imaged with 20x and 60x objectives in an Olympus IX81 inverted fluorescent microscope. At least 30 single cell images were taken for each stiffness and collagen condition.

3.2.2 Endothelial cell morphology measurements

Cell morphology was measured using ImageJ software version 1.44 (NIH free download). Actin fluorescent microscopy images were modified to obtain morphological measurements. First the Gaussian Blur filter (Process – Filter – GaussianBlur, sigma radius = 2 pixels) was used to smooth the grayscale cell image. Then the grayscale image was converted into a binary black and white image using thresholding (Image – Adjust – Threshold). Thresholding defined a grayscale cutoff point, and values below the cutoff became black and values above the cutoff became white. Threshold values were manually adjusted to ensure that the entire cell area was covered. The binary image was used to obtain all morphological factors with the aid of ImageJ particle analyzing plugins. Figure 3.1 below displays sequential image processing.

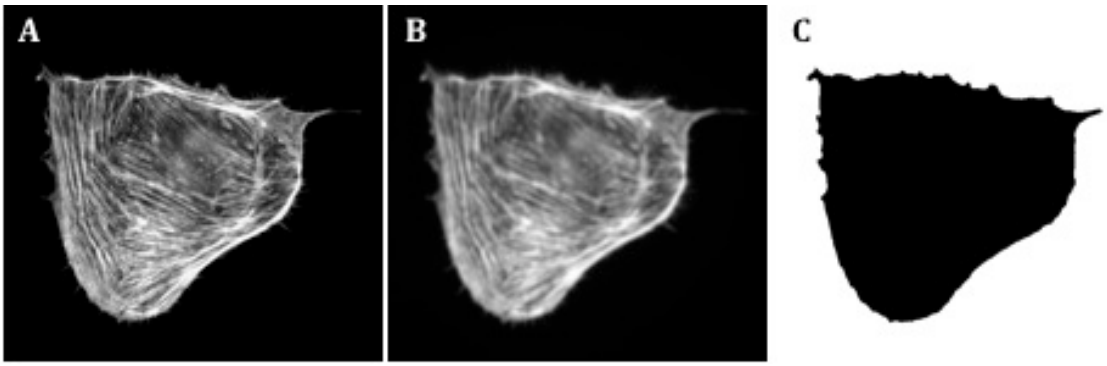

Figure 3.1 Actin gray scale image of a PAEC (A). Gray scale image after smoothing using GaussianBlur tool (B). Binary processed image after thresholding (C). Image C is used to obtain morphological measurement using ImageJ particle analyzing plugins.

Four morphological measurements were recorded:

(1) The cell spread area was calculated as the total area enclosed by the cell boundary.

(2) The cell perimeter was calculated as the length of the cell boundary.

(3) The cell aspect ratio was calculated as the ratio of cell length (fit ellipse major axis) and cell width (fit ellipse minor axis). Values range from 0 to 1 with 1 indicating a perfect circle and 0 indicating an elongated shape.

(4) Cell circularity was defined by the equation 4π*area/perimeter^2. A value of 1.0 indicates a perfect circle. A value approaching 0 indicates an elongated or branched shape.

3.2.3 Endothelial cell focal adhesion number and size

Focal adhesion number was quantified by counting the total number of vinculin spots per cell that were 0.1 – 2 μm^2. Focal adhesion average size was quantified as the average size of the vinculin spots counted within that range. A fluorescent microscopy gray scale image was converted to a binary threshold image using ImageJ (Figure 3.2A). Background subtraction and unsharp masking were used to eliminate background noise. First background noise was eliminated using the Subtract Background tool (Process – Subtract Background; rolling ball radius = 30 pixels) in ImageJ. Then the Unsharp mask tool (Process – Filter – Unsharp Mask; radius = 5 pixels, mask weight = 0.5) was used to help sharpen the image by bringing out the pixels that represented focal adhesion sites.

Finally the grayscale image was converted into binary using the threshold tool (Image – Adjust – Threshold). Figure 3.2 shows the focal adhesion image processing sequence. Unsharp masking was of particular importance before image thresholding to identify focal adhesion sites.

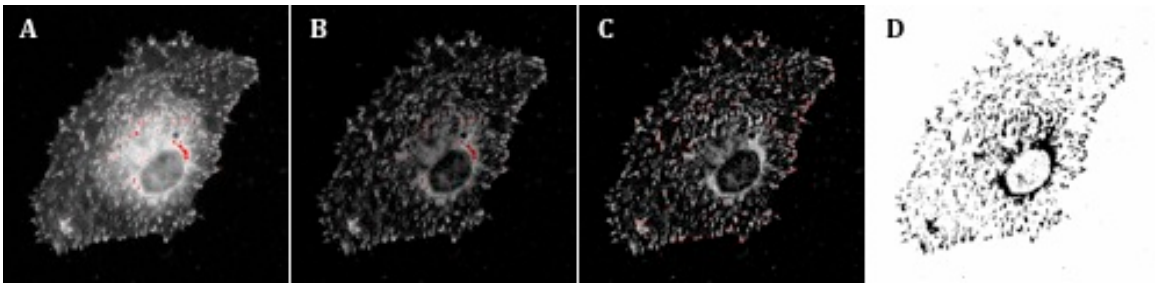

Figure 3.2 Focal adhesion image processing from grayscale to binary. (A): unprocessed grayscale image of focal adhesion sites on a cell. (B): grayscale image after background noise is reduced. (C): grayscale after it has been sharpened using the Unsharpmask tool. (D): binary image after thresholding showing focal adhesion sites in black

3.2.4 Statistical Analysis

Statistical analysis was done with Excel's data analysis toolbox. Data were graphed as mean ± standard deviation. Comparisons between two groups (e.g., 0.3 kPa NC vs. 0.3 kPa GC) were analyzed by Student's *t*–test and comparisons among multiple groups were performed by one-way Analysis of Variance (ANOVA). $p < 0.05$ was considered statistically significant. Number of samples analyzed varied from 15 to 40 unless otherwise specified.

3.3 Results

3.3.1 Endothelial cell images

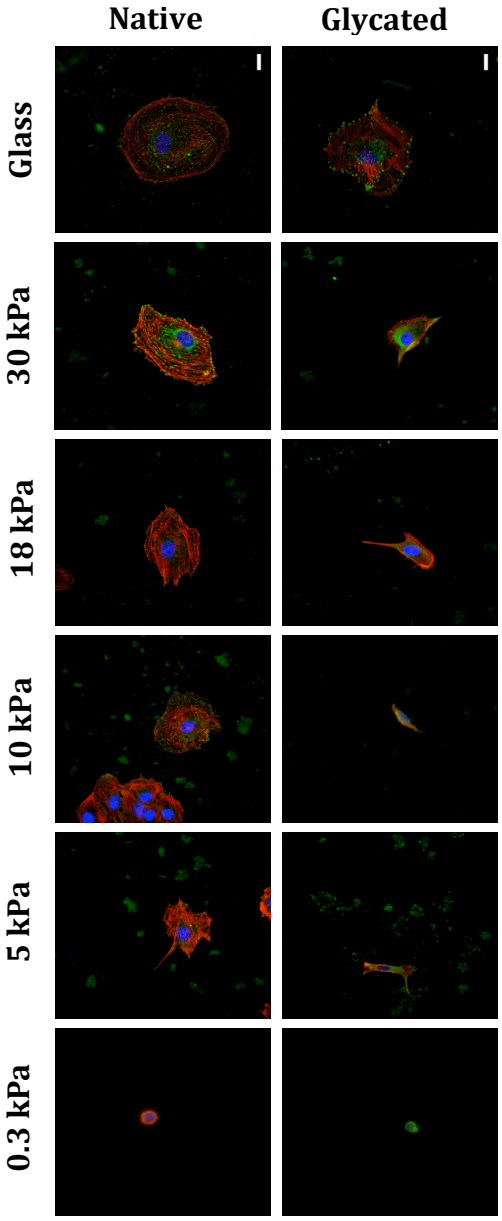

Figure 3.3 On native collagen, PAEC show more actin fibers and focal adhesion formation as stiffness increases; this trend is not as apparent in cells on glycated collagen. Fluorescent images of PAEC seeded on: soft PA gels (G = 0.3 kPa), physiological stiffness PA gels (G = 5 kPa, 10 kPa), stiff PA gels (G = 18kPa, 30 kPa) and glass. Cells were labeled for F-actin (red), vinculin (green) and nuclei (blue). Scale bar = 20 μm.

Endothelial cells were previously shown to increase spread area with substrate stiffness. Our goal was to determine if this trend was maintained when cells were seeded on an ECM protein that was altered by a disease environment. We therefore compared endothelial cell morphology on PA gels and glass coated with native and glycated collagen.

Figure 3.3 shows the variation in cell morphology on native and glycated collagen as substrate stiffness increased from soft (0.3 kPa) all the way up to glass stiffness. On native collagen, PAEC area increased with stiffness; F-actin stress fibers and focal adhesion sites also became more organized as stiffness rose. On glycated collagen, PAEC showed limited F-actin stress fiber organization and focal adhesion assembly when compared to cells on native collagen at the same substrate stiffness. Interestingly, cells on glass showed similar morphology and cytoskeletal organization when cultured on both native and glycated collagen.

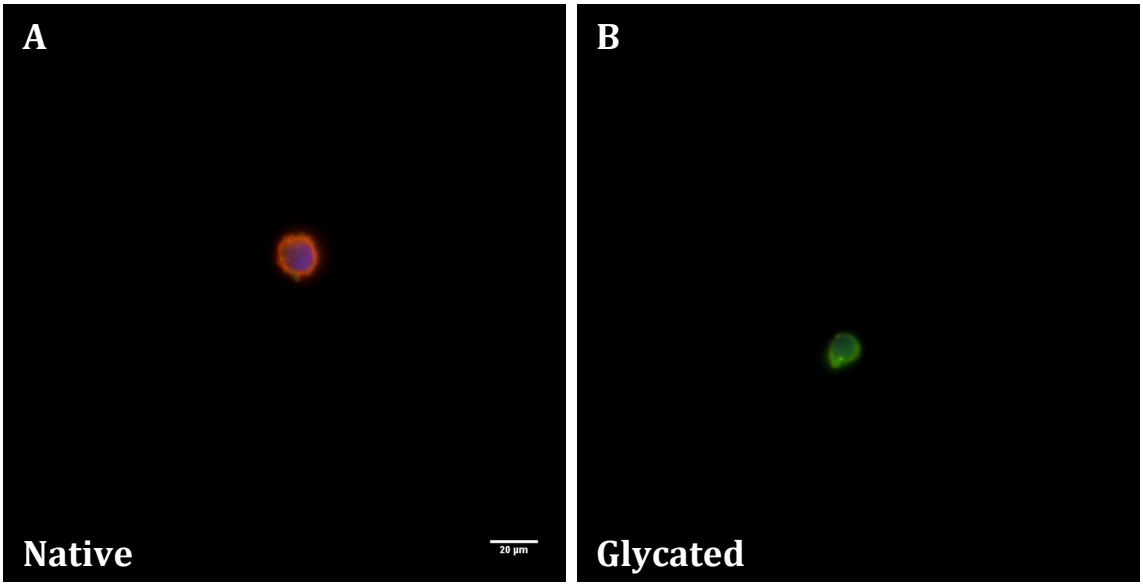

Figure 3.4 Cells on both native (A) and glycated (B) collagen coated 0.3 kPa gels showed little spreading or actin fiber formation. Cells were labeled for F-actin (red), vinculin (green) and nuclei (blue). Scale bar = 20 µm.

For the most compliant gel (0.3 kPa, Figure 3.4), cells on native and glycated collagen exhibited similar morphological features including area and aspect ratio. At this stiffness, cells showed little to no actin filament or focal adhesion organization.

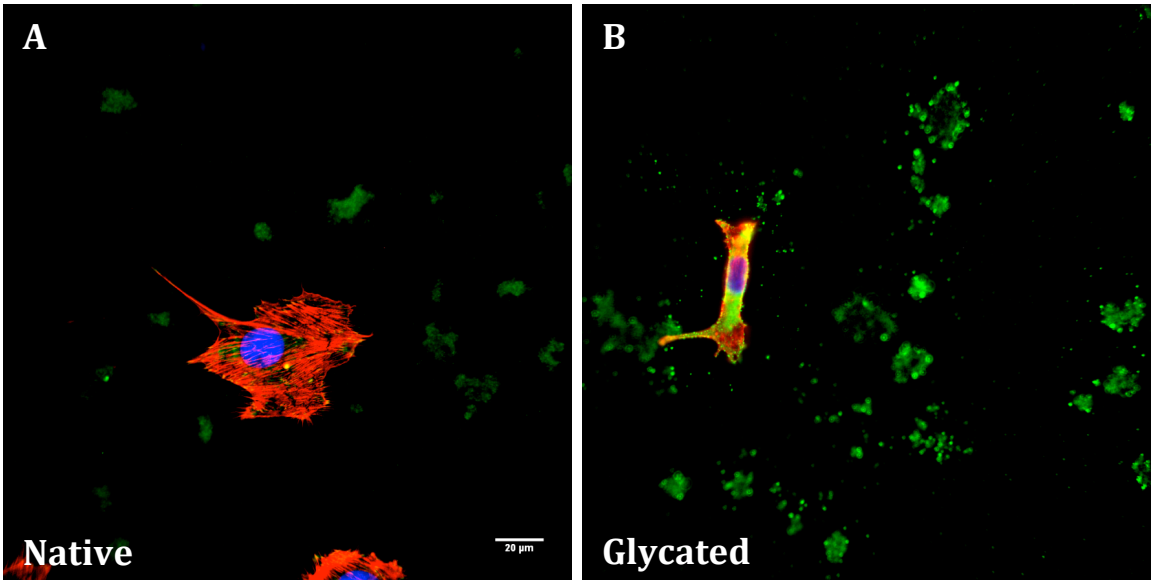

Figure 3.5 On 5 kPa gels, cells on native collagen (A) had larger spread area and showed more developed F-actin fibers than cells on glycated collagen (B). Cells were labeled for F-actin (red), vinculin (green) and nuclei (blue). Scale bar = 20 µm.

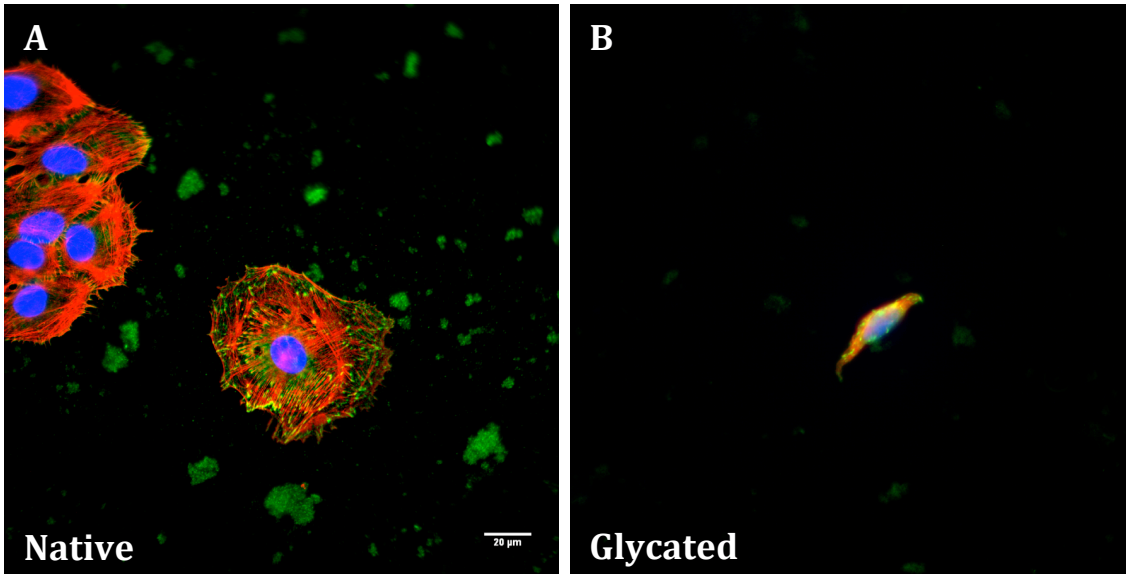

Figure 3.6 On 10 kPa gels, cells on native collagen (A) had larger spread area and showed more developed F-actin fibers than cells on glycated collagen (B). Cells were labeled for F-actin (red), vinculin (green) and nuclei (blue). Scale bar = 20 µm.

For gels of physiological stiffness (5 and 10 kPa), cells on native collagen showed a more developed actin cytoskeleton network, with thicker and thus possibly more mature actin stress fibers, as well as more organized focal adhesion sites that occurred at the ends of actin filaments (Figures 3.5 and 3.6). Cells on glycated collagen coated gels (5 and 10 kPa) still were not able to effectively organize actin filaments and focal adhesions.

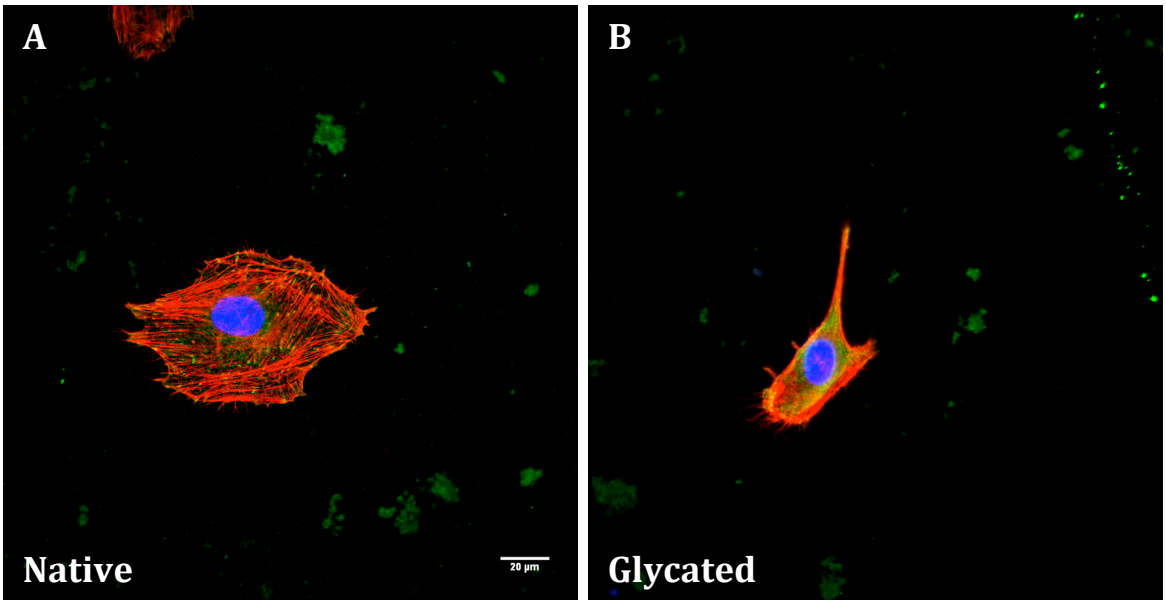

Figure 3.7 On 18 kPa gels, cells on native collagen (A) showed more developed F-actin stress fibers and focal adhesion formation compared to cells on glycated collagen (B). Cells were labeled for F-actin (red), vinculin (green) and nuclei (blue). Scale bar = 20 µm.

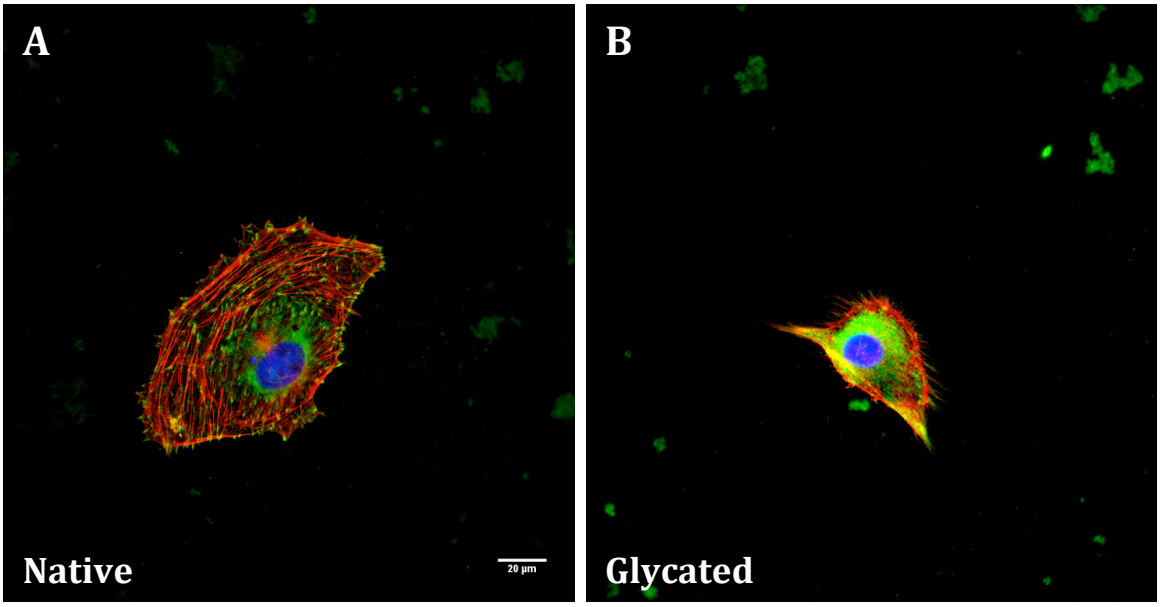

Figure 3.8 On 30 kPa gels, cells on native collagen (A) showed more developed F-actin stress fibers and focal adhesion formation compared to cells on glycated collagen (B). Cells were labeled for F-actin (red), vinculin (green) and nuclei (blue). Scale bar = 20 µm.

Figures 3.7 and 3.8 show cell morphological response to stiffer substrates (18 and 30 kPa). Cells on gels coated with native collagen had thicker F-actin fibers reminiscent of stress fibers. Consequently, cells had a more spread morphology and defined focal adhesions at the ends of actin filaments. Cells seeded on glycated collagen coated gels showed less F-actin and focal adhesion organization compared to cells on native collagen at the same stiffness. However, these cells did have higher spread area and subsequently more developed F-actin organization compared to cells on the lower stiffness gels (0.3, 5 and 10 kPa).

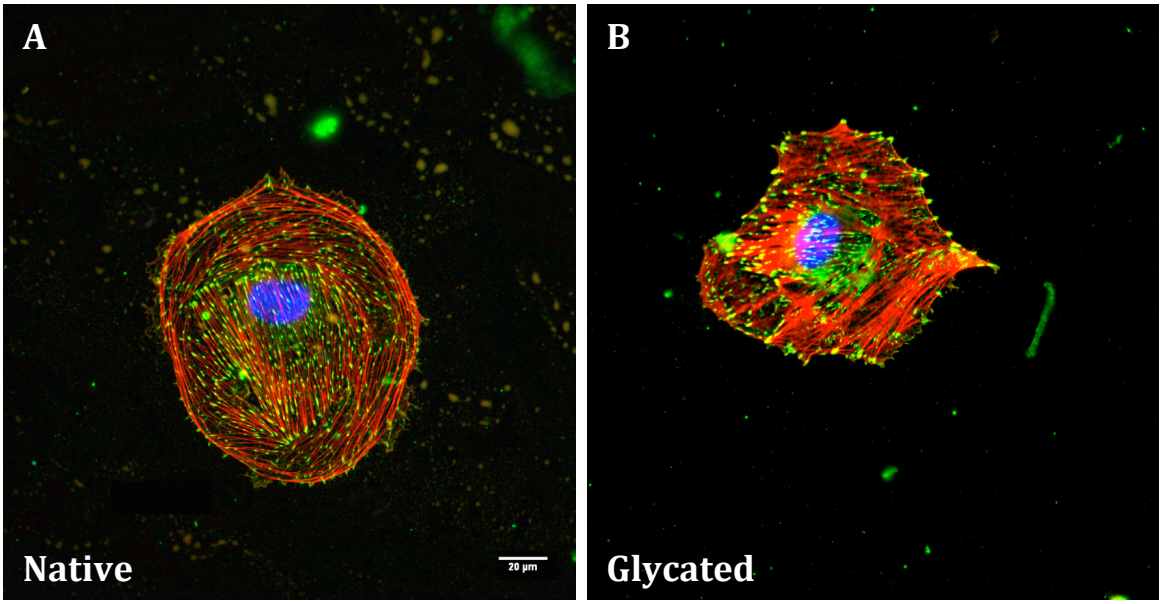

Figure 3.9 Cell on native (A) and glycated (B) collagen coated glass showed little difference in morphology, F-actin, and focal adhesion organization. Cells were labeled for F-actin (red), vinculin (green) and nuclei (blue). Scale bar = 20 µm

PAEC on both native and glycated collagen coated glass (Figure 3.9) are highly spread and display well-developed stress fibers and focal adhesion sites. No clear morphological difference was observed among cells cultured on native and glycated collagen coated glass.

3.3.2 Quantitative analysis of cell morphology

Morphological differences among cells on native and glycated collagen coated gels of increasing stiffness were quantitatively analyzed.

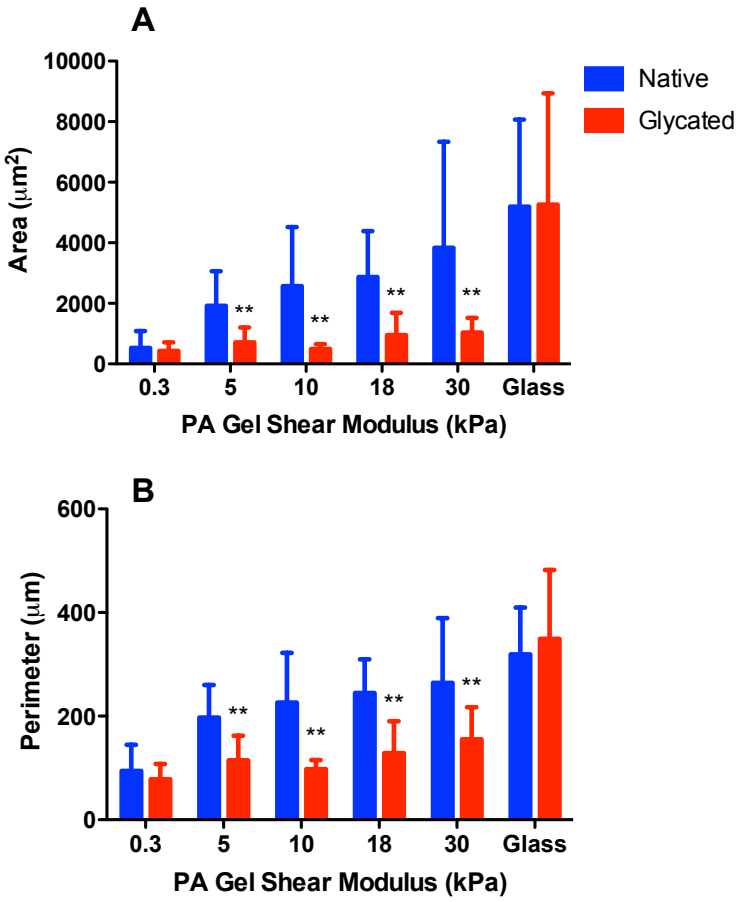

*Figure 3.10 Cell area (A) and perimeter (B) increased with substrate stiffness on both native and glycated collagen coated substrates ($p < 0.01$ by ANOVA). However, at each stiffness level, cells on native collagen showed higher area and perimeter. (**$p < 0.01$ compared to native of same stiffness by Students t-test). Error bars indicated standard deviation.*

Cell area and perimeter were analyzed to determine the degree of cell spreading. Cells on glass had the highest area (~5500 μm^2) and perimeter (~400 μm) for native as well as glycated collagen substrates. At the other end of the spectrum, cells on the most

compliant gels (0.3 kPa) had the lowest area (~500 μm^2) and perimeter (~100 μm), and these values were similar for both native and glycated collagen substrates. Between 0.3 kPa and glass, both cell area and perimeter increased as a function of stiffness on native and glycated collagen coated substrates ($p < 0.01$ by ANOVA). Cells on 30 kPa gels had similar perimeter values compared to cells on glass but statistically significant different values for area ($p < 0.05$ by Student t-test). Cells on glycated collagen had lower cell area and perimeter than cells on native collagen for 5, 10, 18, and 30 kPa gels ($p < 0.01$).

The change in cell area and perimeter with substrate stiffness on both native and glycated collagen were quantified using a curve fit (Figures 3.11 and 3.12). A one-phase exponential curve fit produced R^2 values of 0.9681 for area and 0.9901 for perimeter for cells on native collagen and R^2 values of 0.7601 for area and 0.8589 for perimeter for cells on glycated collagen.

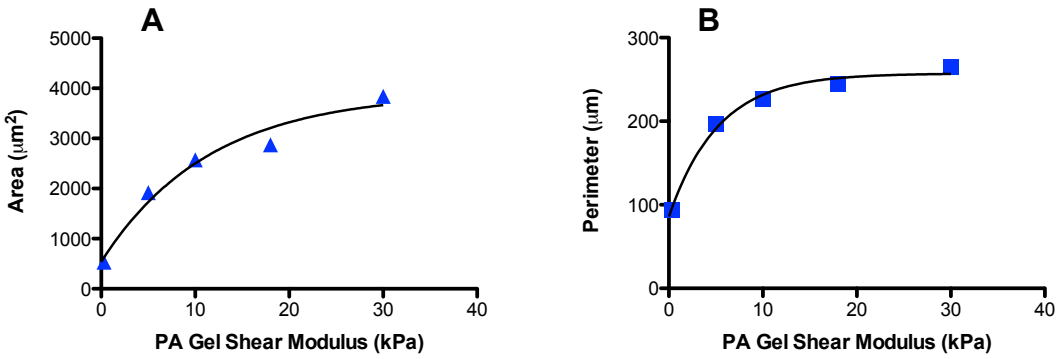

Figure 3.11. Curve fits of area (A) and perimeter (B) vs. substrate shear modulus for cells on native collagen. One-phase exponential fit. Area: $R^2 = 0.968$. Perimeter: $R^2 = 0.9901$.

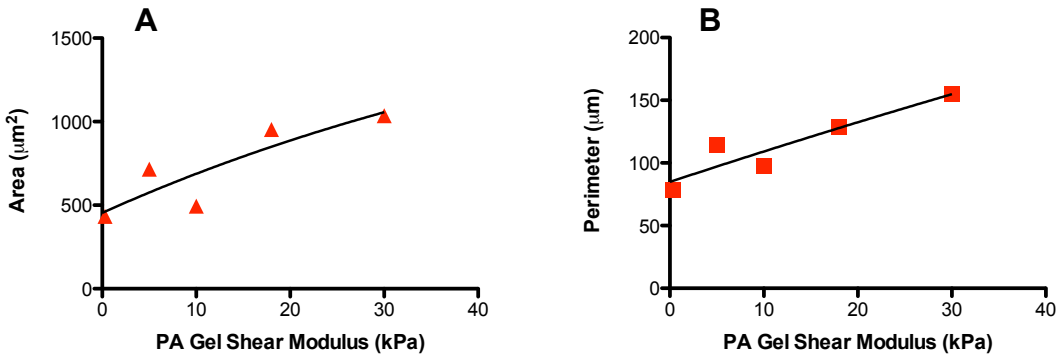

Figure 3.12. Curve fit of area (A) and perimeter (B) vs. substrate shear modulus for cells on glycated collagen. One-phase exponential curve fit. Area: $R^2 = 0.7601$. Perimeter: $R^2 = 0.8589$.

Cell aspect ratio and circularity were analyzed for cells on both native and glycated collagen coated substrates of different stiffness to quantify the effect on cell shape. Cell aspect ratio, defined as the ratio of cell length to cell width, on native collagen remained relatively constant (~1.6) as stiffness increased (Figure 3.13A). On glycated collagen, cell aspect ratio increased significantly ($p < 0.05$ by Student's *t*-test) from ~1.3 on 0.3 kPa to ~1.6 on 5 kPa. Compared to native collagen, cell aspect ratio was only significantly lower on glycated collagen on the most compliant gel. For all other stiffnesses, cell aspect ratio on glycated collagen was similar to that of cells on native collagen.

Circularity reflects the similarity of an object shape to that of a circle. Values range from 0 to 1, with 1 representing a perfect circle and values less than 1 representing branched shapes. Circularity was highest (~0.8) for cells on 0.3 kPa gels for both native and glycated collagen coatings (Figure 3.13B). Cell circularity decreased significantly for both substrate coatings ($p < 0.01$ by Student's *t*-test) as stiffness increased to 5 kPa (~0.6) and then remained relatively constant as substrate stiffness increased further.

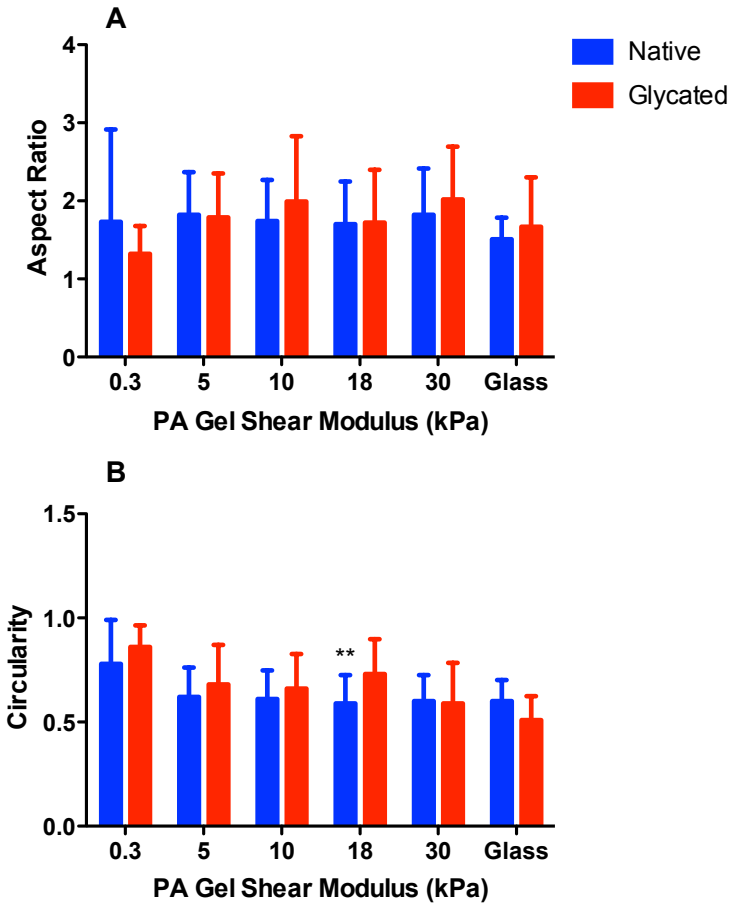

*Figure 3.13. Cell shape indices for PAEC on PA gels and glass coated with native and glycated collagen did not exhibit consistent trends. (A) Aspect ratio, (B) circularity. (**p < 0.01 compared to native of same stiffness by Students t-test). Error bars indicated standard deviation.*

3.3.3 Focal adhesion size and number

Cell response to substrate stiffness most likely emerges at cell-substrate adhesion sites where substrate properties are mechanotransduced [6]. To determine if changes in cell morphology correlated with changes in focal adhesions, we quantified focal size and number in cells on native and glycated substrates of different stiffness. On the 0.3 kPa PA substrate, there were no visible focal adhesions in cells on either native or glycated

collagen, thus no measurements were done at this stiffness. Average focal adhesion size was significantly lower ($p < 0.05$ by Student *t*-test, 5 kPa glycated vs. Glass glycated) with ~0.3 μm^2 for cells on 5 kPa glycated collagen coated substrates and highest (~0.6 μm^2) for both native and glycated collagen coated glass. Between 5 kPa and 18 kPa, the average vinculin size remained fairly constant (~0.5 μm^2) on native collagen-coated gels but then increased significantly ($p < 0.05$ by Student's *t*-test, 18 kPa native vs. 30 kPa native) at 30 kPa and Glass. Focal adhesion size was consistently lower for cells on glycated collagen compared to native collagen, except on glass.

Focal adhesion number on native collagen was smallest at 5 kPa with ~250 focal adhesion sites per cell. Focal adhesion number increased with substrate stiffness more than 100% up to ~580 sites for cells on 30 kPa gels and glass. For cells on glycated collagen, focal adhesion number was lowest (~50 focal adhesion sites per cell) for cells on gels in the physiological stiffness range (5 and 10 kPa). Focal adhesion number more than doubled for gels of 18 and 30 kPa stiffness and was highest for cells on glass. The number of focal adhesions was consistently lower for cells on glycated collagen coated gels, but was similar for cells on both native and glycated collagen coated glass.

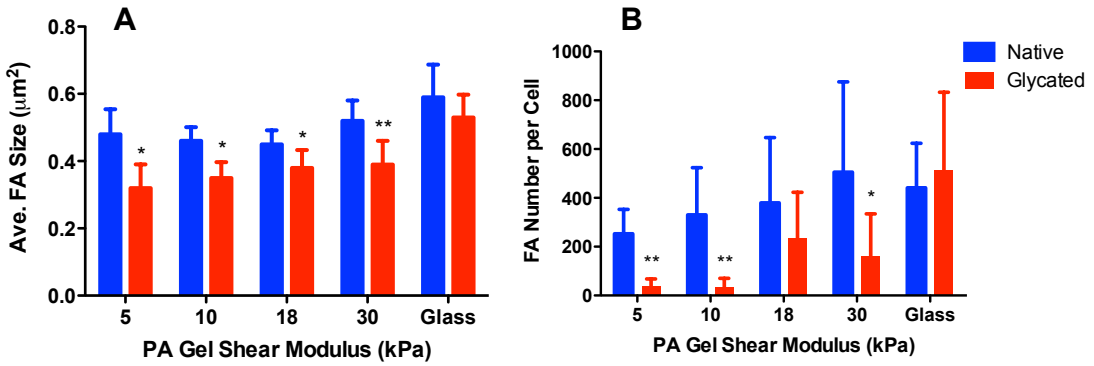

Figure 3.14 Focal adhesion size (A) did not change with gel stiffness but did increase on glass, and focal adhesion number (B) increased with stiffness on both native and glycated collagen coated substrates ($p < 0.01$ by ANOVA). Focal adhesion size and number were consistently lower in cells on glycated collagen compared to native collagen ($p < 0.05$, **$p < 0.01$ compared to native of same stiffness by Students t-test)*

Focal adhesion size and number were plotted vs. average cell area to determine the linear dependence among these variables using the Pearson product-moment correlation coefficient (Figure 3.15). The correlation was only significant between focal adhesion number and cell area in cells on native collagen ($r = 0.9992$). The correlation study is summarized in Table 3.1.

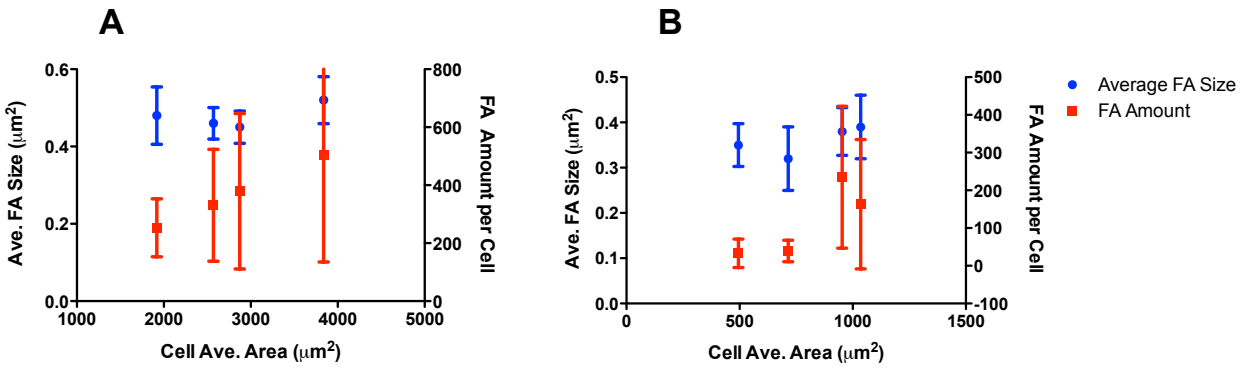

Figure 3.15. Focal adhesion size and number compared to average cell area on native (A) and glycated (B) substrates. Only focal adhesion number in cells on native collagen increased linearly with cell area (R^2 = 0.998).

Table 3.1 Pearson product-moment correlation analysis for focal adhesion size and number vs. cell area for native and glycated-coated substrates.

	Native, NC		Glycated, GC	
	Average FA Size	FA Number	Average FA Size	FA Number
Pearson r	0.5922	0.9992	0.7143	0.8463
P value (two-tailed)	0.4078	0.0008	0.2857	0.1537
P value summary	ns	***	ns	ns
Is the correlation significant? (alpha=0.05)	No	Yes	No	No
R squared	0.3508	0.9984	0.5102	0.7162

3.3.4 50:50 native and glycated collagen coated substrates

PAEC were cultured on PA substrates of different stiffness coated with a 50:50 ratio of native and glycated collagen to determine if cell response to substrate stiffness would be more similar to cells on native or glycated collagen coated substrates. Cells on 50:50

native:glycated collagen looked similar to cells on 100% native collagen when their morphology and cytoskeleton were qualitatively observed by immunofluorescent microscopy (Figure 3.16). F-actin fiber and focal adhesion organization were not well developed for cells on the lowest stiffness gels. However, the cytoskeleton became more organized as substrate stiffness increased.

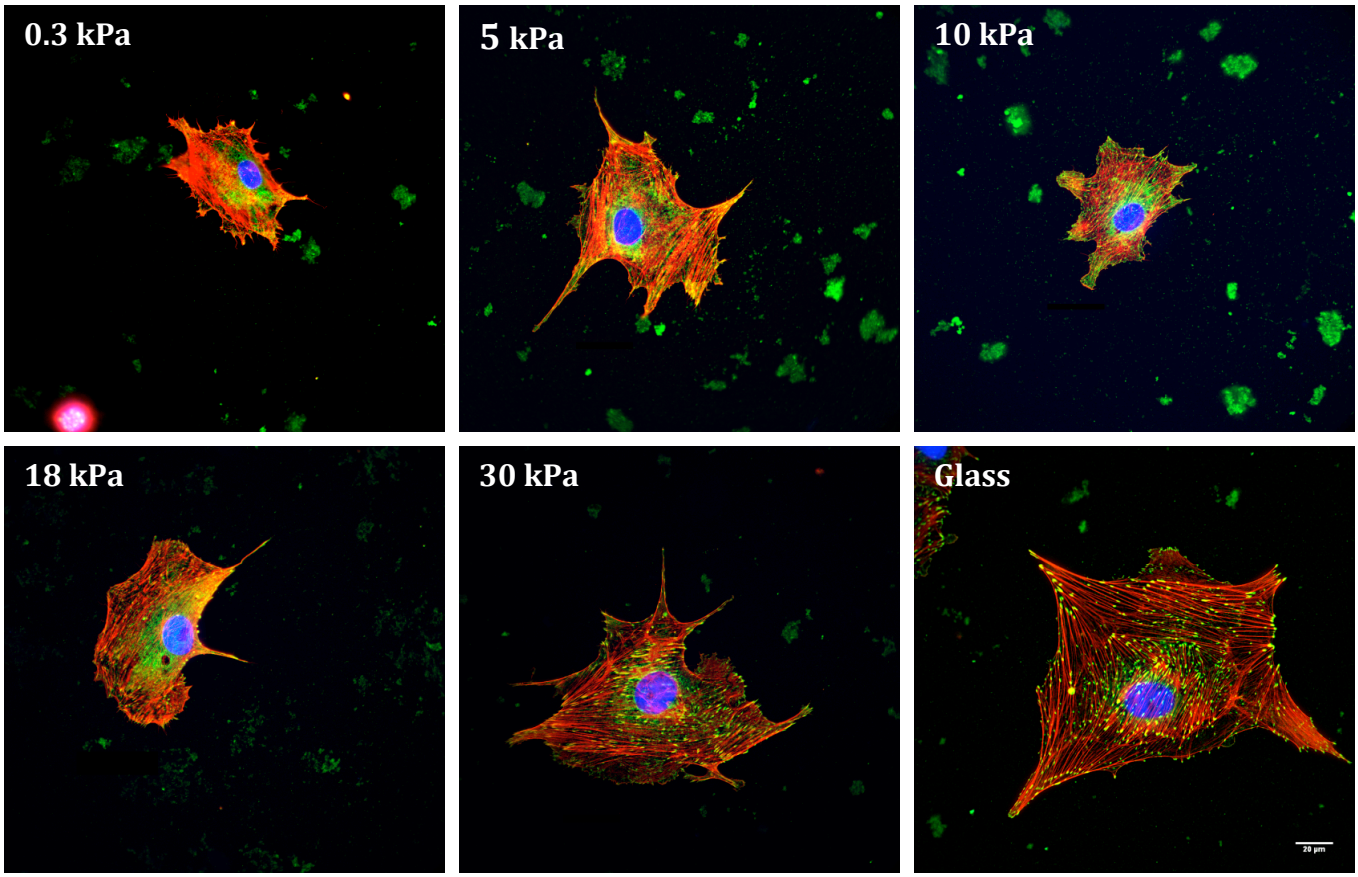

Figure 3.16 Fluorescent images of PAEC seeded on 50:50 native:glycated collagen coated gels. Cell area as well as actin fiber and focal adhesion formation at the individual stiffnesses looked similar to that of cells on native collagen. Cells were labeled for F-actin (red), vinculin (green) and nuclei (blue). Scale bar = 20 μm

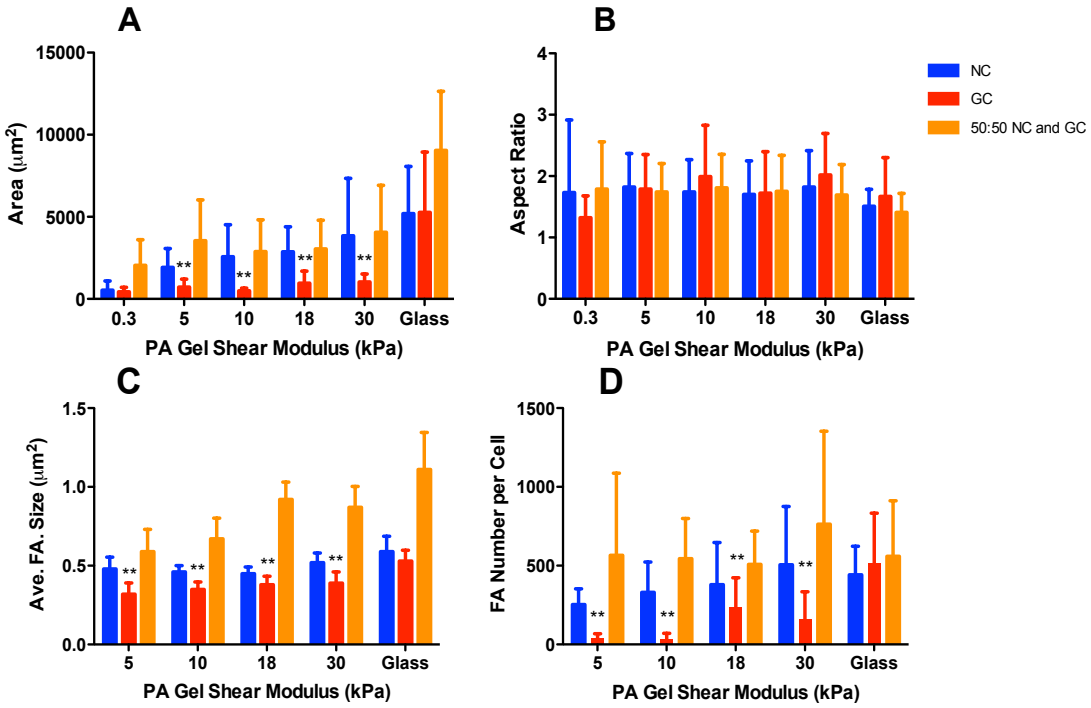

*Figure 3.17 Cells on 50:50 native and glycated collagen substrates were similar in morphology and focal adhesion formation to cells on native collagen substrates. A: Cell area. B: Cell aspect ratio. C: Focal adhesion number and D: Focal adhesion size. (*p < 0.05 and **p < 0.01 compared to 50:50 native:glycated collagen data by Students t-test)*

Cells on 50:50 native and glycated collagen substrates exhibited similar spread area, aspect ratio, FA amount and size to cells on native collagen (Figure 3.17). Cell spread area was similar for all stiffness values except 0.3 kPa and glass, for which area was significantly higher compared to both native and glycated collagen substrates. Focal adhesion size and number in cells on 50:50 native and glycated collagen were also similar to cells on native collagen for all stiffness values. Cells on glycated collagen were statistically significantly different from cells on 50:50 native:glycated collagen at most stiffnesses and for most measurements.

3.4 Discussion

Understanding cell-ECM interactions is crucial to cell migration, growth and differentiation. Cell morphology and cytoskeletal structure are key outputs of cell-ECM interactions. ECM stiffness varies in physiological settings and increases with aging [30] and diseases such as diabetes [31]. In this study, we determined the effect of both substrate stiffness and glycated collagen coating on cell morphology and cytoskeletal structure. Previous studies showed that endothelial cell spread area increased with substrate stiffness [5, 7] but cells on glycated collagen did not spread properly [25]. We now show that PAEC increase their spread area and focal adhesion number as substrate stiffness increases from 0.3 kPa to glass. Cell area and focal adhesion number were higher for cells on native compared to glycated collagen on all substrates from 5 kPa to 30 kPa. These data suggest that cells sense substrate stiffness more effectively on native collagen compared to glycated collagen, thus allowing them to spread and develop more organized stress fibers and focal adhesions.

Endothelial cell area and consequently perimeter increased with substrate stiffness on both native and glycated collagen coated substrates. These data are similar to previous studies in which cell area increased with substrate stiffness [5, 7, 8, 13]. Mechanotransduction, the process by which cells sense and respond to mechanical changes in their environment, involves integrins that form a direct link between ECM proteins and the cell cytoskeleton [32]. This interaction can be classified as a force balance in which integrins maintain stability between tensile actin fibers and ECM anchorage points [29]. Early studies suggest that changing the ECM stiffness disrupts this force balance thus directly regulating actin cytoskeleton assembly and contractility [8,

33]. For cells to spread on a given substrate, the high forces exerted by tensile actin fibers need to be balanced by high substrate forces. Soft substrates cannot resist the high cell tension, thus cells on softer substrates are smaller and more rounded.

On glycated collagen, cell area was significantly lower compared to cells on native collagen at each gel stiffness. I believe this behavior is related to the integrins cells use to attach to the native vs. glycated collagen. Endothelial cells use $\alpha_1\beta_1$ and $\alpha_2\beta_1$ integrins to bind to the GFOGER sequence of native collagen fibrils [34]. Glycated collagen alters collagen structure, which may interfere with $\alpha_2\beta_1$ binding since the collagen glycation site is only 10 nm away from the integrin binding site [35]. Cells could use alternative integrins other than $\alpha_2\beta_1$ to bind to glycated collagen [27]. Many mechanotransduction responses, including endothelial cell response to shear stress, are integrin dependent. Thus cells on glycated collagen may not be able to sense substrate stiffness due to altered integrin attachment.

However, on glass substrates, cell area was similar between cells on native and glycated collagen. This can be explained by the fact that glass is infinitely stiffer compared to gels, and cells are unable to sense changes in stiffness above 300 kPa. At glass stiffness, cells may be able to exert higher forces on both native and glycated coated substrates even if they use an alternative integrin to bind to glycated collagen.

Cell spread area and perimeter increased exponentially for cells on native collagen in response to PA substrate stiffness, reaching a plateau by about 30 kPa. These data suggest that cell sensing of substrate stiffness has a threshold, above which increased stiffness no longer has an effect. Cell area and perimeter on glycated collagen substrates did not show

a similar plateau. Thus glycated collagen could change or even remove the substrate stiffness threshold effect, perhaps through altered integrin interactions.

Cell response to substrate stiffness on gels coated with 50:50 native and glycated collagen was similar to that of cells on native collagen coated substrates. These data suggest that in an environment where both native and glycated collagen are present, PAEC prefer to attach to native collagen perhaps due to the $\alpha_2\beta_1$ integrin binding sites.

3.5 Conclusion

I now show that glycated collagen disturbed endothelial cell morphological response to PA substrates of different stiffness. While PAEC on native collagen increased in size as substrate stiffness increased, this effect was smaller in PAEC on glycated collagen. The change in cell morphology correlated with changes in cytoskeletal and focal adhesion organization. These data bring new understanding to endothelial cell dysfunction in a diabetic environment. Collagen glycation both changes its biochemical interactions with cells as well as the ECM stiffness through enhanced crosslinking. This study suggests that these two changes with glycated collagen may have integrated effects on cells.

In the next chapter, I further study cell force generation on native and glycated collagen coated substrates of different stiffness by measuring the traction forces that cells generate.

4 Endothelial Cell Traction Forces

4.1 Introduction

In Chapter 3, I showed increased cell area and focal adhesion formation as PA substrates coated with native or glycated collagen increased in stiffness. However, the increase in cells on glycated collagen was significantly smaller compared to cells on native collagen. These results suggest that cells on glycated collagen are not as mechanosensitive to substrate stiffness as cells on native collagen possibly due to a change in integrin attachment.

Cell traction forces (CTFs) and stiffness are of great importance for cells. When cell attach to the ECM, they generate internal tensile forces through actin-myosin interactions which in turn exert tractions on the ECM. Cells use traction forces for migration, cell shape maintenance and other functions essential for their survival [12]. The relationship between CTFs and cell stiffness with PA substrate stiffness has been established. For example, bovine aortic endothelial cells seeded on PA substrates coated with collagen increased traction force significantly as stiffness increased from 1 to 10 kPa [7]. Similarly, fibroblasts increased in stiffness from 6 to 8 kPa when seeded on 20 kPa gels and glass [15]. However, it is not known how PAEC stiffness and traction stresses vary in response to substrate stiffness in a diseased state.

In this chapter, I explore how collagen glycation affects endothelial cell traction forces and cell stiffness in response to increasing substrate stiffness. Cell traction force was measured using traction force microscopy (TFM), and cell stiffness was measured using

atomic force microscopy methods (AFM). In the following sections, the methods used to pattern and analyze the cell traction forces as well cytoskeleton stiffness are explained along with the results of the study and the difficulties encountered.

4.2 Methods

4.2.1 PA gel micropatterning

Tetramethylrhodamine-labeled bovine serum albumin (TMR-BSA, Invitrogen) was patterned onto a thin PA gel (0.25 mm thick) using an indirect patterning technique (Figure 4.1). First, 10 mg/ml Biotin XX (Invitrogen) in sterile dimethylsulfoxide (DMSO) was added to 2 mg/ml TMR-BSA in PBS for a final concentration of 2 mg/ml biotin TMR-BSA. The solution was vortexed gently for one hour. Biotin TMR-BSA was aliquoted into sealed protein filter cartridges (Ambion) and stored overnight at 4°C to remove excess TMR-BSA to remove BSA that did not bind to the biotin solution. The biotin TMR-BSA solution was removed from the protein filter cartridges and stored at -20°C for future use.

PDMS stamps of 2.5 μm diameter circles separated by 15 μm were used for surface patterning. First, 0.07 mg/ml biotin TMR-BSA in PBS was adsorbed onto the PDMS stamp for 40 minutes. Excess fluid was then removed from the stamp using a filtered air gun. Finally, the stamp was brought into contact with a glass coverslip (Figure 4.1). A 1 mg weight was placed on top of the stamp to enhance contact with the glass. After 7 minutes, the stamp was removed.

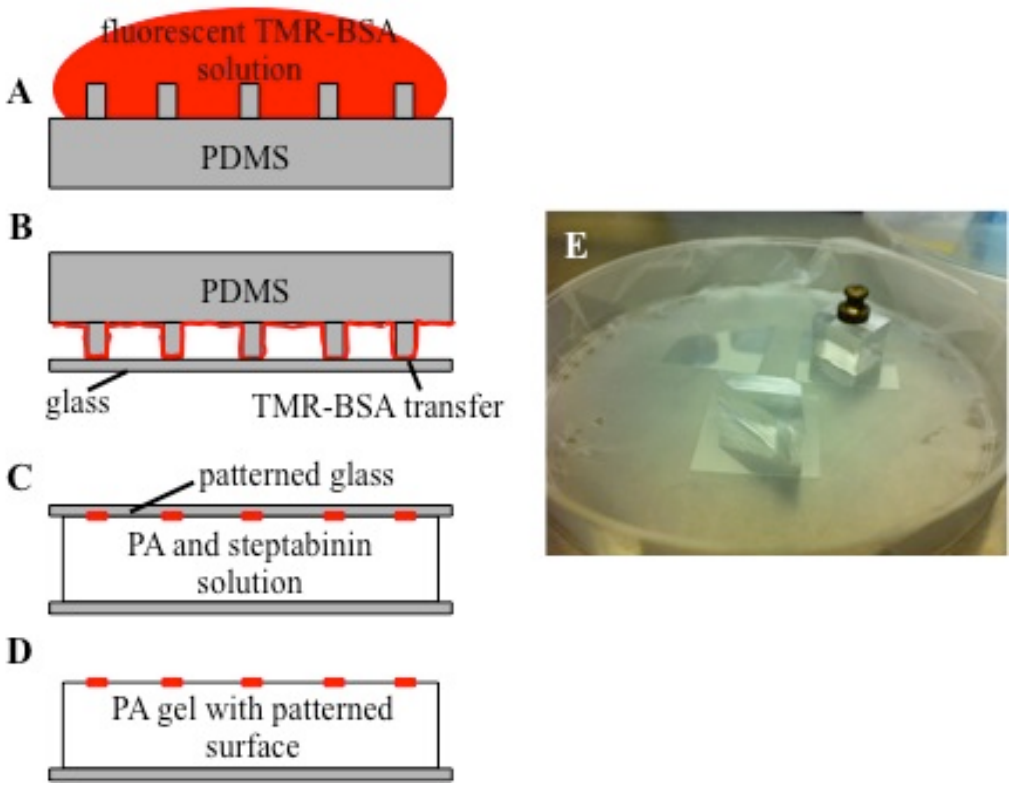

Figure 4.1 Process of making patterned gels using a PDMS stamp. (A): fluorescently labeled BSA was adsorbed onto a plasma-treated stamp. (B): BSA was stamped onto a glass coverslip. (C): the glass coverslip was placed on a PA gel pre-polymer. (D): the top coverslip was removed and the pattern was transferred to the gel. (E): Photograph of glass coverslip stamping.

To transfer the pattern onto a PA gel, a hydrophilic glass coverslip was prepared as previously described in Section 2.2.2. 5 µl of 2 mg/ml streptavidin acrylamide (Invitrogen) was added to 100 µl PA solution. Streptavidin acrylamide was added to the PA solution to bind the biotin TMR-BSA to the gel surface. Next 0.35 µl tetramethylethylenediamine (Fisher) and 1 µl 10% ammonium persulfate (Fisher) were added sequentially to polymerize the gel. 100 µl streptavidin PA solution was added to the hydrophilic bottom coverslip, and the stamped coverslip was immediately put onto the PA solution to create a sandwich as illustrated in Figure 4.1. The PA gel was

polymerized between the two coverslips for 60 minutes in a PBS bath to keep the gel moist. After 60 minutes, the top glass coverslip was removed and the gel was washed three times with PBS for 5 minutes. The gels were then conjugated with native or glycated collagen and cells were seeded as explained in Chapters 2 and 3.

4.2.2 Endothelial cell traction stress measurement

A total of three images were needed to obtain the traction stress field for each individual cell using the LIBTRC 2.4 software. The first image was a phase contrast image of the cell to outline the boundary of the cell. The second and third images were fluorescent images of the dot pattern with no cell (null pattern) and the dot pattern after being deformed by the cell (stressed pattern).

The null patterned image was taken from a gel area that did not have cells on it. This image was then stacked and aligned with the cell-deformed stress patterned image using the ImageJ plugin, Align Slices in Stack [36]. The dot displacement field and traction stresses generated by the cell were calculated using the LIBTRC 2.4 software developed by Micah Dembo of Boston University [11] with a regularization factor λ equal to 0. Due to time and material constrains we were only able to successfully calculate traction forces for one cell per individual stiffness on each collagen condition.

4.2.3 Endothelial cell cytoskeleton stiffness

Cell stiffness was measured using an atomic force microscope. The cell was analyzed with a Bioscope (Veeco, Woodbury, NY) mounted on a microscope (Eclipse TE200-U, Nikon) using silicon nitride cantilevers (205 μm long, 25 μm wide, 0.6 μm thick) with a

pyramid tip. The cantilever's spring constant, provided by the manufacturer, was 0.06 N/m and it was used for all calculations (DNP-10, Bruker). The cell was indented at three distinct locations, with the average from those three measurements defined as the cell stiffness. The stiffness of the gel adjacent to the cell was also measured.

To calculate stiffness, the first 200-300 nm of tip deflection from the horizontal (Δd) was fit with the Hertz model modified for a cone [37].

$$\Delta d = \frac{k}{4A} + \Delta z + \frac{1}{2}\sqrt{\left(\frac{k}{A}\right)^2 + 4\frac{k\Delta z}{A}} \quad \text{and}$$

$$A = \frac{2}{\pi}\tan(\alpha)\frac{E}{1-\upsilon^2} \tag{4.1}$$

where k and Δz are the cantilever bending rigidity and vertical indentation; E is Young's modulus; α is the cone tip angle; and υ is the Poisson ratio. Young's modulus is the ratio between the strains ($\delta z/z$). The Poisson ratio is defined as the ratio of compression strain in the direction normal to the applied stress and the extensional strain in the direction of the applied stress and is taken to be 0.5 for all samples.

4.3 Results

4.3.1 Micropattern transfer to PA gel

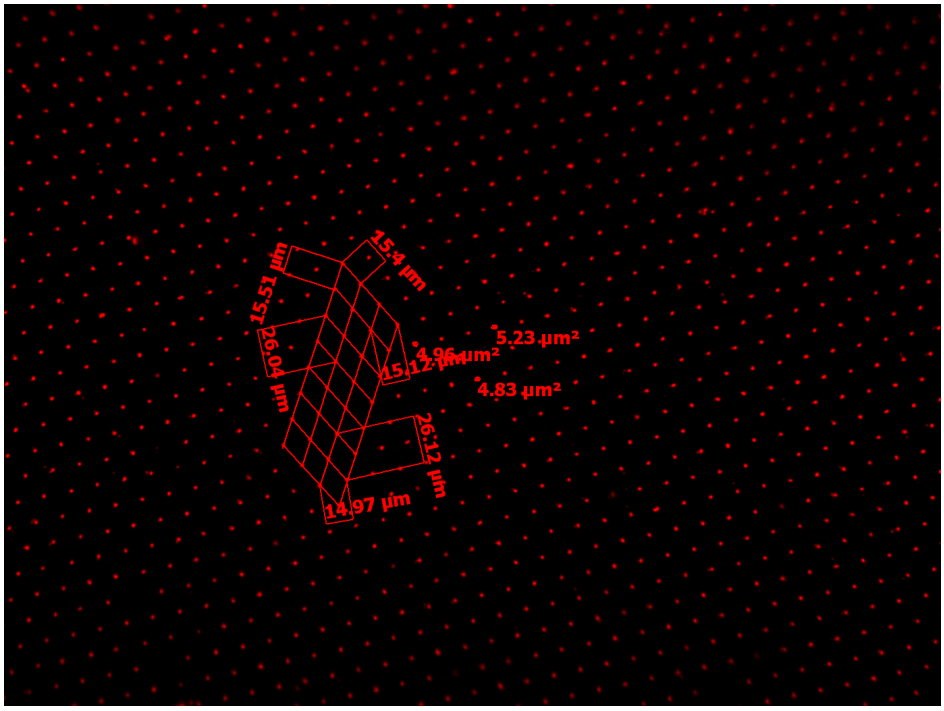

Figure 4.2 Tetramethylrhodamine-labeled bovine serum albumin (TMR-BSA) micropattern transferred onto PA gel using a PDMS stamp.

TMR-BSA micropatterns were successfully transferred on PA gels using a pattern stamped coverslip (Figure 4.2). Measurements of three random patterned dots revealed an average area of 5.01 µm^2, a diameter of 2.53 µm, and distance between dots of 15.29 µm. These measurements are close to the original PDMS stamp, which had 2.5 µm diameter circular patterns spaced 15 µm apart.

4.3.2 Endothelial traction force microscopy

PAEC traction forces on 1.8, 5 and 10 kPa PA gels coated with native or glycated type I collagen were obtained by measuring the deformation of a patterned grid of dots.

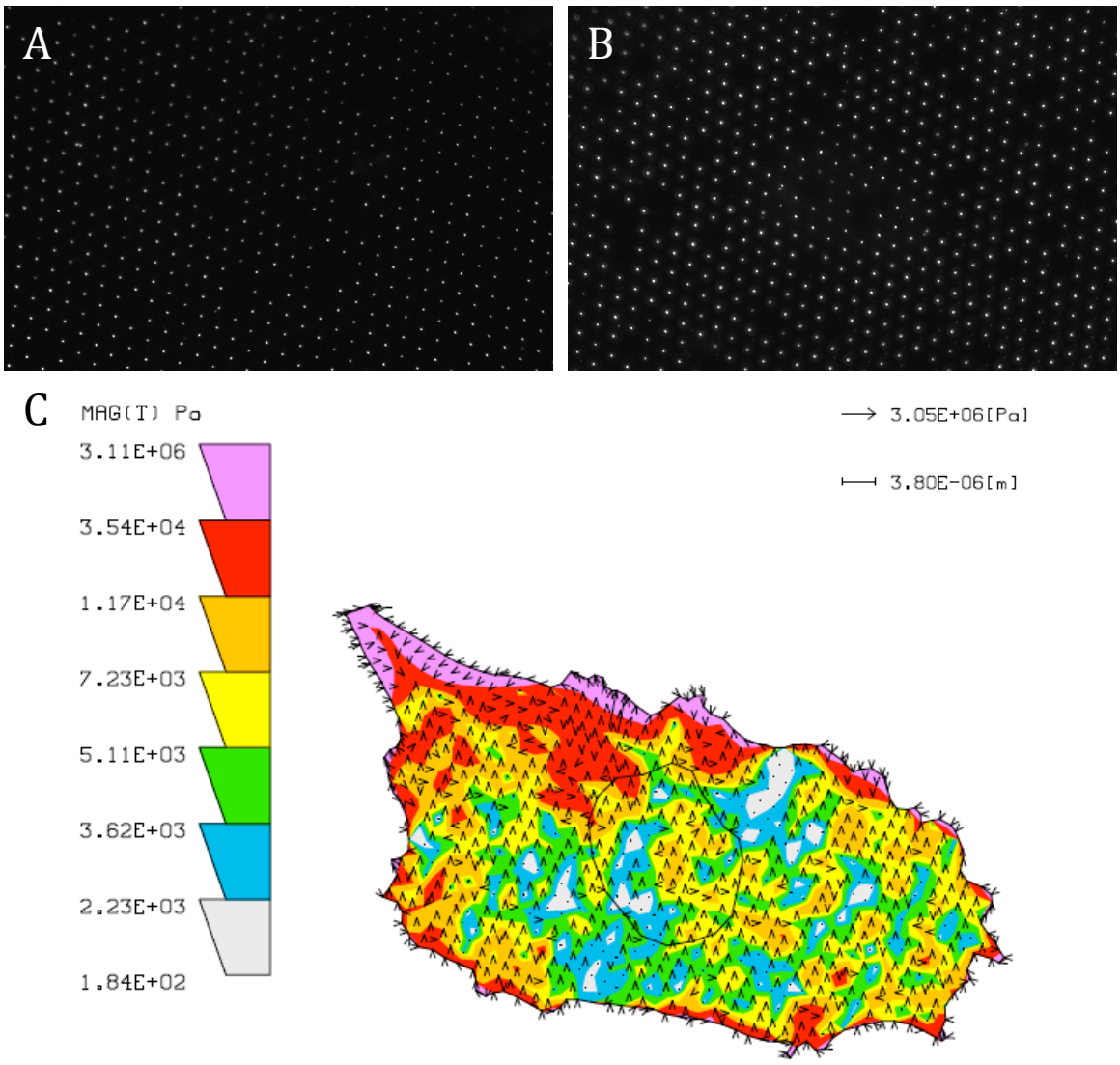

Figure 4.3 Traction force measurement of PAEC on 1.8 kPa gel coated with native collagen. (A): Fluorescent image of the null pattern. (B): Fluorescent image of the cell stressed patterned dot grid. (C): Cell traction heat map with stress magnitude and direction.

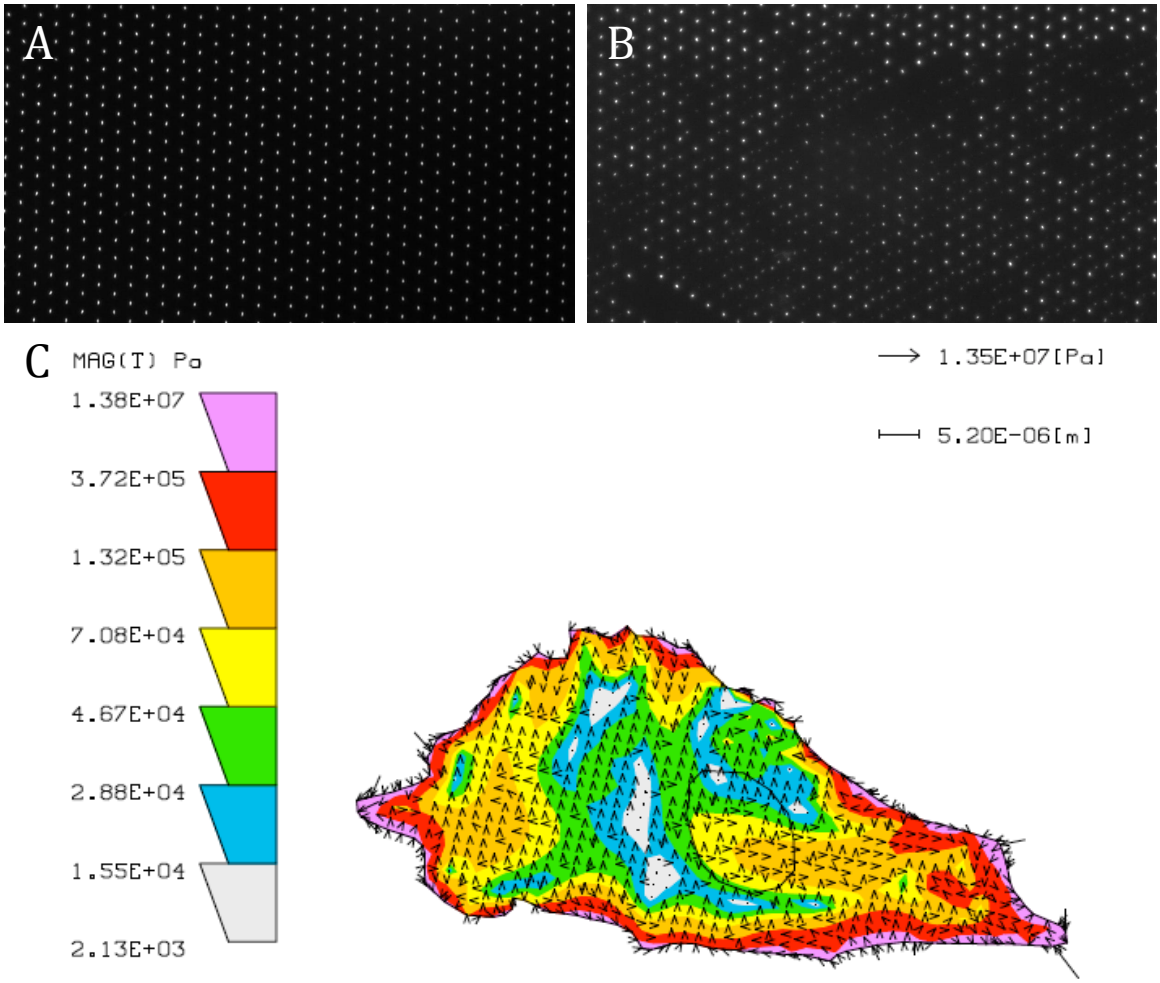

Figure 4.4 Traction force measurement of PAEC on 5 kPa gel coated with native collagen. (A): Fluorescent image of the null pattern. (B): Fluorescent image of the cell stressed patterned dot grid. (C): Cell traction heat map with stress magnitude and direction.

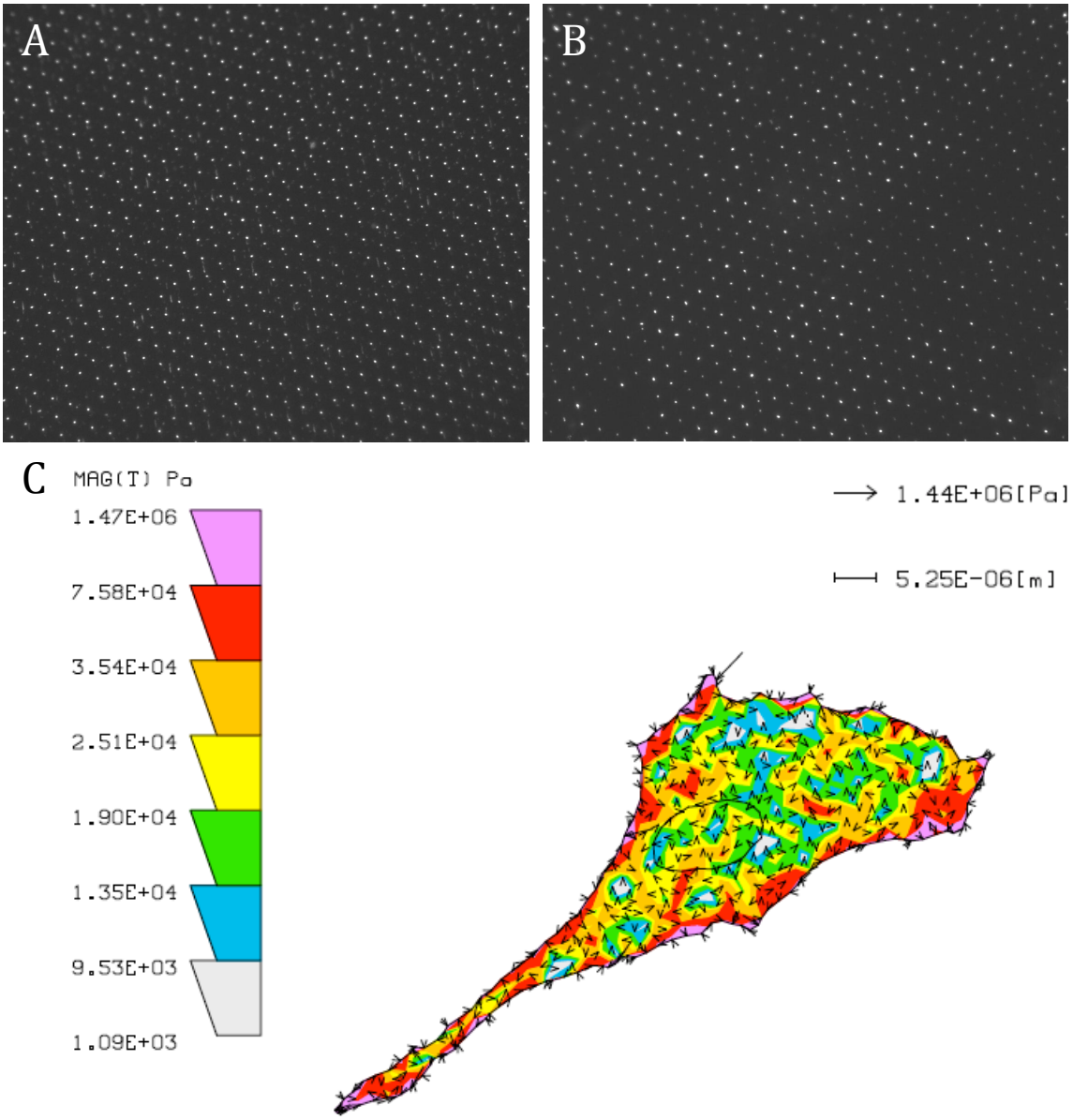

Figure 4.5 Traction force measurement of PAEC on 10 kPa gel coated with native collagen. (A): Fluorescent image of the null pattern. (B): Fluorescent image of the cell stressed patterned dot grid. (C): Cell traction heat map with stress magnitude and direction.

Figures 4.3 through 4.5 display the traction fields exerted by cells on 1.8, 5 and 10 kPa gels coated with native collagen, respectively. In all three cells on native collagen coated substrates, the maximum traction stress occurred at the cell periphery and pointed towards the cell nuclei. The maximum cell traction stress was highest in cells on the 5 kPa gel and lower in cells on the 1.8 and 10 kPa gels. On the 1.8 kPa gel, the maximum and minimum stresses recorded were 3.11×10^{06} Pa and 1.84×10^{02} Pa, respectively. On the 5 kPa gel, the maximum and minimum stresses recorded were 13.8×10^{06} Pa and 21.3×10^{02} Pa, respectively. On the 10 kPa gel, the maximum and minimum stresses recorded were 1.47×10^{06} Pa and 10.9×10^{02} Pa, respectively.

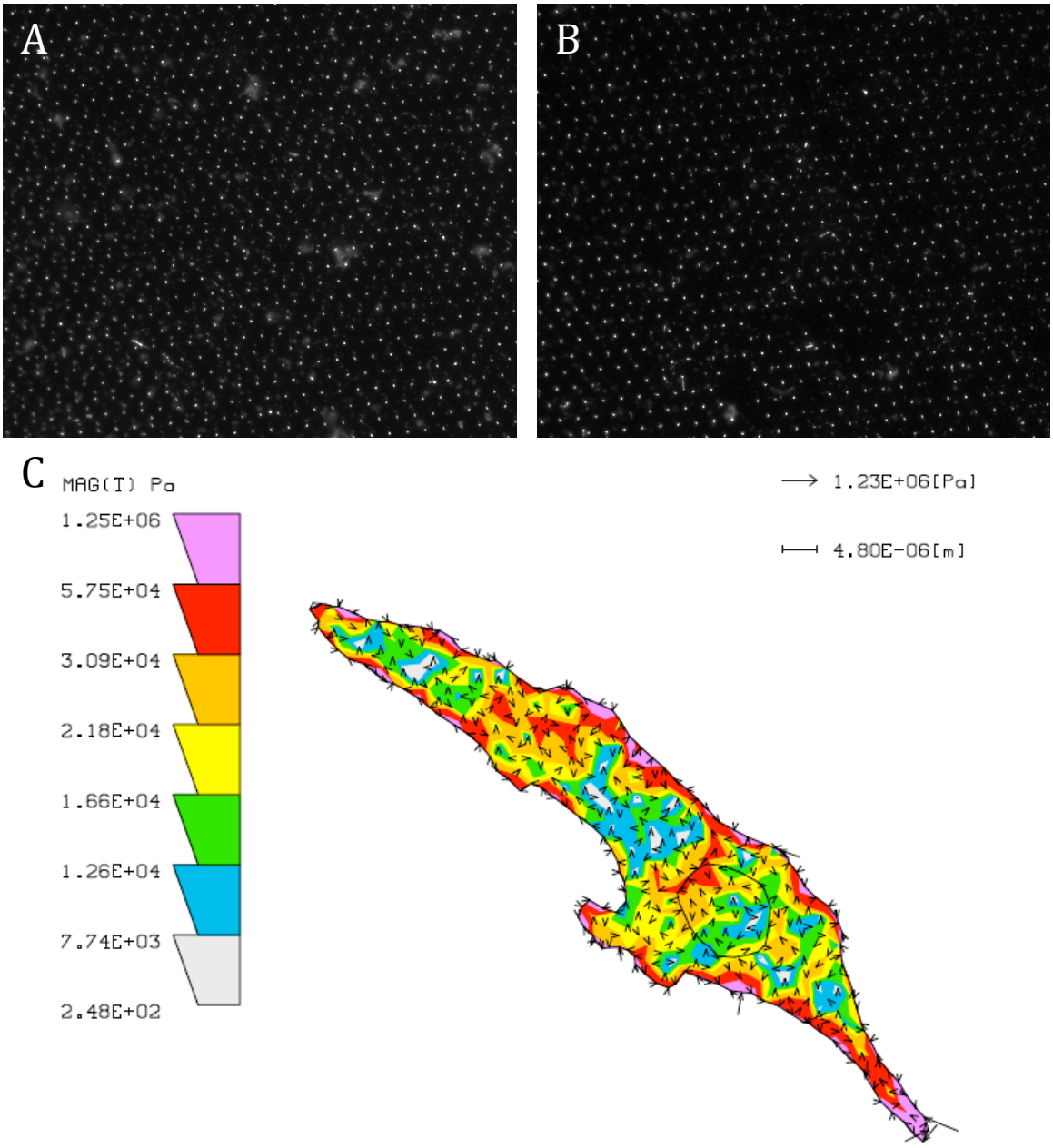

Figure 4.6 Traction force measurement of PAEC on 5 kPa gel coated with glycated collagen. (A): Fluorescent image of the null pattern. (B): Fluorescent image of the cell stressed patterned dot grid. (C): Cell traction heat map with stress magnitude and direction.

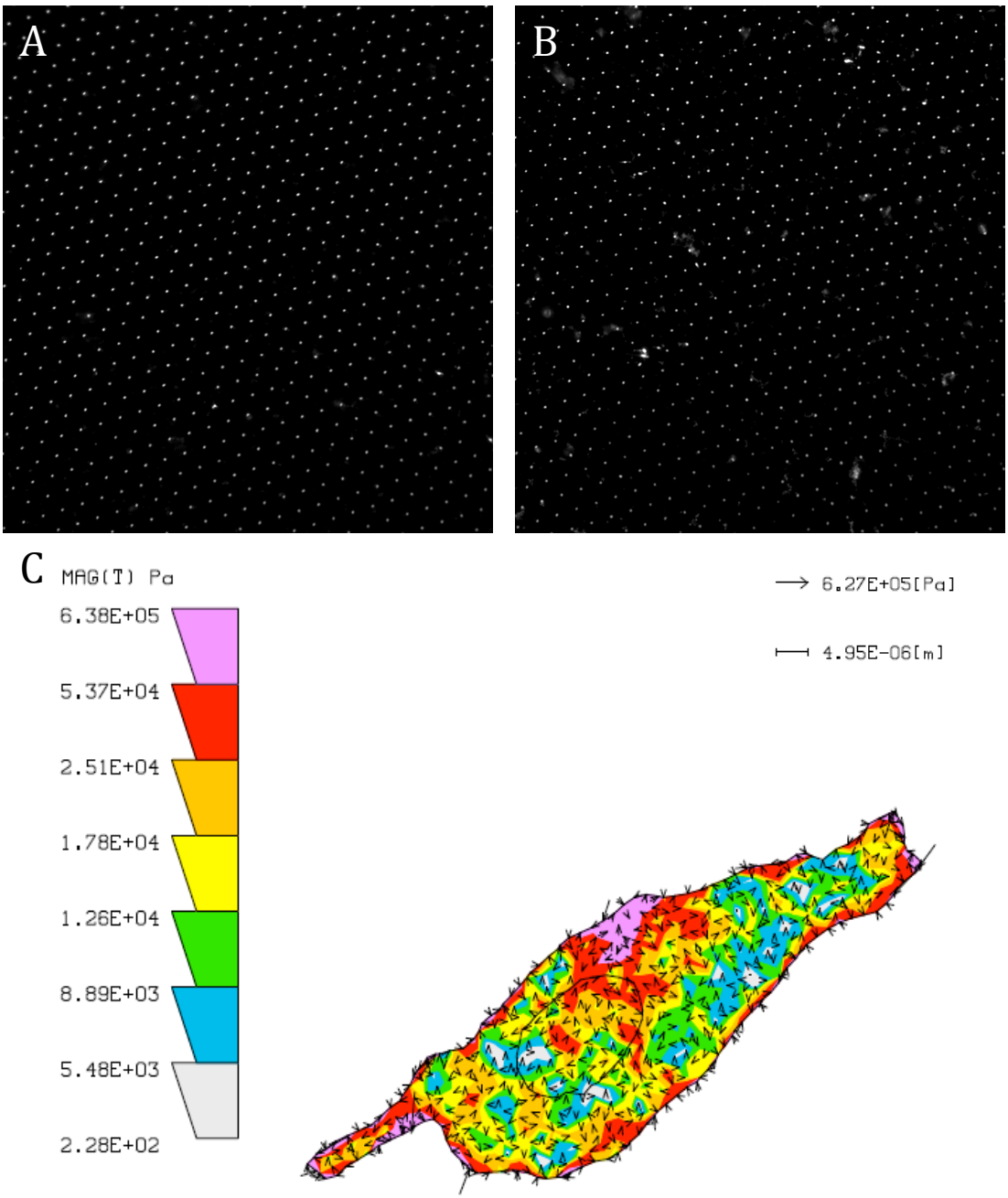

Figure 4.7 Traction force measurement of PAEC on 10 kPa gel coated with glycated collagen. (A): Fluorescent image of the null pattern. (B): Fluorescent image of the cell stressed patterned dot grid. (C): Cell traction heat map with stress magnitude and direction.

Figures 4.6 and 4.7 displays the traction fields exerted by cells on 5 and 10 kPa gels coated with glycated collagen. The cells on these two gels exhibited maximum traction stress at the cell periphery and pointed towards the cell nuclei. The maximum cell traction stress was highest at 5 kPa gel and lower at 10 kPa gels. On the 5 kPa gel, the maximum and minimum stresses recorded were 1.25×10^{06} Pa and 2.48×10^{02} Pa, respectively. On the 10 kPa gel, the maximum and minimum stresses recorded were 0.638×10^{06} Pa and 2.28×10^{02} Pa, respectively.

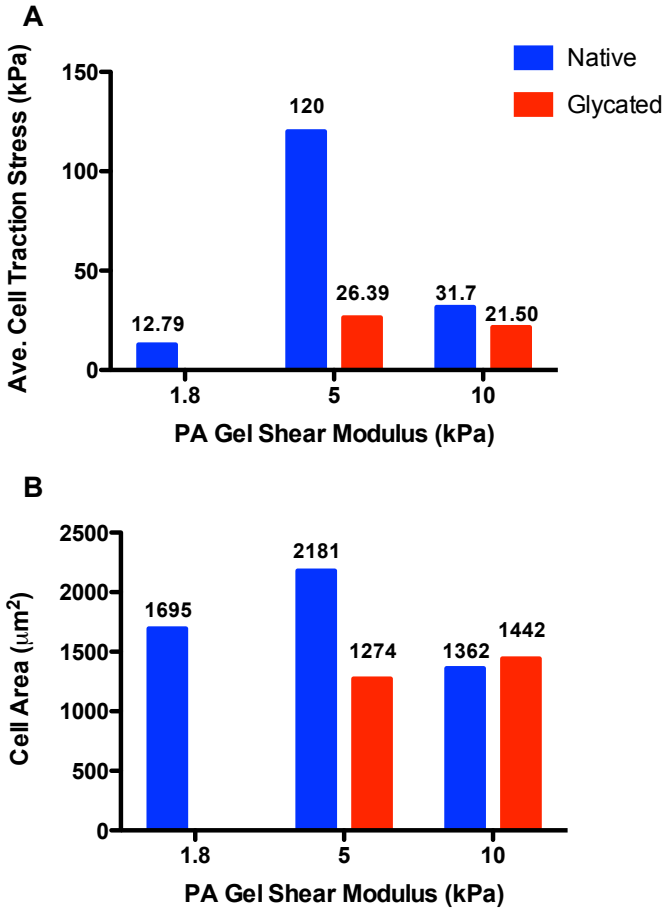

Figure 4.8 Average cell traction (A) and cell area (B) for cells seeded on native and glycated collagen coated gels of different stiffness computed using the LIBTRC 2.4 software.

For the native collagen coated gel, the lowest average traction stress (12.79 kPa) was recorded at the lowest substrate stiffness (1.8 kPa, Figure 4.8A). Average cell traction stress for the cells on 5 and 10 kPa gels was over 800% higher for the 5 kPa gel and over 100% higher for the 10 kPa gel compared to the cell traction stress on the 1.8 kPa gel. On glycated collagen coated substrates, the average cell traction stress was similar for 5 kPa and 10 kPa gels (only 18% difference). On the 5 kPa gel, the average cell traction stress was 78% higher on native compared to glycated collagen. On the 10 kPa gel, the average cell traction stress was 33% higher on native compared to glycated collagen.

Cell area was also measured (Figure 4.8B). Cell area on native collagen substrates was highest at 5 kPa (2181 μm^2) and lowest at 10 kPa (1362 μm^2). On glycated collagen coated substrates, cell area was similar at 5 kPa (1274 μm^2) and 10 kPa (1442 μm^2). Cell area on native collagen compared to glycated collagen coated gels was 42% higher for 5 kPa but similar for 10 kPa (6% difference).

4.3.3 Endothelial cell stiffness

Endothelial cell stiffness was measured for PAEC seeded on 5 and 10 kPa PA substrates as well as glass substrates coated with native and glycated collagen. On both native and glycated collagen, the highest cell stiffness was recorded on glass (~9 kPa) while the lowest cell stiffness (~5 kPa) was recorded on the 5 kPa gels. There was no statistical significant difference (by one-way ANOVA or by Student's *t*-test) between cells on native and glycated collagen. The only statistically significant difference was for cells on the 5 kPa gel as compared to glass on native collagen.

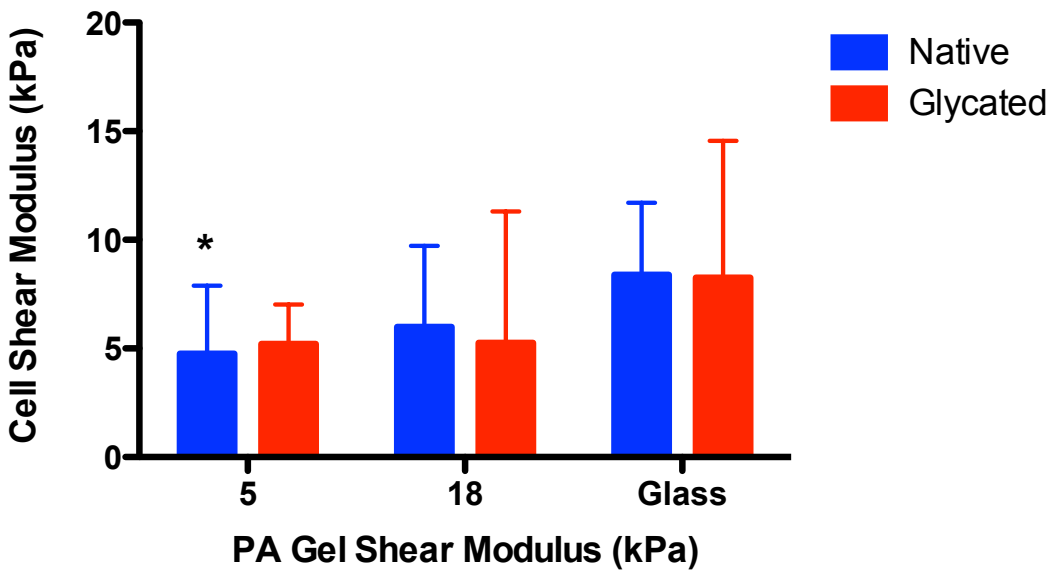

*Figure 4.9 Endothelial cell shear modulus of elasticity increased on glass as compared to PA gels. (*p < 0.05 compared to glass on native collagen by Student's t-test). Error bars indicate standard deviation. Number of samples was between 6 and 16.*

4.4 Discussion

Cell traction forces are essential to cell migration and shape maintenance, and cell stiffness is critical to cell response to applied mechanical forces. The results presented here are preliminary since new protocols to measure CTF and stiffness were used for the first time in our lab. Our results indicated that PAEC traction stresses on native collagen overall increased with substrate stiffness, which agrees with previous studies [38]. On glycated collagen substrates, CTF was overall lower than in cells on native collagen coated gels of the same stiffness. These data fit well with the reported decrease in cell area and FA formation on glycated collagen substrates in Chapter 3. Thus our CTF results suggest that endothelial cells are not able to transmit traction forces to the glycated

collagen substrate, which may lead to decreased cell spreading. This is important because we now have identified that on glycated conditions cells are not able to properly transmit forces to the substrate to which they attach, and this may prevent them from reaching spread areas similar to cells seeded on native collagen environments.

Conventional TFM methods use fluorescent beads embedded on PA substrates to measure substrate deformation caused by cell traction forces [11]. The bead fields are imaged before (stressed configuration) and after cell removal (relaxed configuration). This method although already proven to be successful in its objective can be time and material consuming as only one or two images of individual cells can be captured per PA substrate. In an effort to address these and other issues we adopted a new approach of tracking PA substrate deformation. Instead of using bead fluorescent markers, we used a grid of fluorescent dots patterned onto the surface of PA gels. This allowed us to fix cells using 4% paraformaldehyde in their contractile state and thus compare multiple cell-deformed images with a cell undeformed grid per PA substrate. The dots were patterned using fluorescently labeled BSA. BSA was ideal in our case because it allowed native and glycated collagen to be conjugated across the entire PA surface using sulfo-SANPAH as previously described in section 2.2.

This new method was not quite as accurate as desired. Cell attachment caused the dots not only to change position but also change shape from circular to oval. Thus some of the accuracy in measuring actual dot marker position change might have been lost in the analysis as the traction stress that went into dot deformation was never captured by this software. Also, blank spots where the pattern was not completely transferred to the PA surface might also contribute to loss of traction stress information. The calculated CTF

range was significantly higher (from 12 to 120 kPa on substrates varying from 1.8 to 10 kPa stiffness) than reported values for endothelial cells seeded on the same PA stiffness range (from 300 to 1000 Pa) [7]. However, our calculated stiffness could be adjusted by varying the regularization factor λ used in Dembo's analysis. Finally, an additional error could have occurred in 10 kPa gel coating. Since these cells had roughly the same spread area in traction force experiments (but not in cell morphology experiments), these conditions should be repeated.

Cell stiffness measurements using atomic force microscopy also yielded inconclusive results; however several trends matched well with the literature and our cell area data. Cells on glass exhibited the largest stiffness (~9 kPa), a value that is similar to stiffness of fibroblasts on glass [15]. Cell stiffness was the same on glass for both native and glycated collagen conditions, which correlates with similar values for cell area and FA formation in cells on native and glycated collagen glass presented in Chapter 3. At lower PA stiffnesses (5 and 18 kPa), cell stiffness decreased in cells on both native and glycated collagen but the change was not statistically significant compared to cells on glass. At each individual substrate stiffness, there was also no statistically significant difference in cell stiffness for samples on native and glycated collagen. This results did not agree with previous data showing that cell area and FA formation along with CTF were lower on glycated compared to native collagen coated substrates. Thus more experiments are needed to clarify the relationship between PAEC stiffness and PA substrate stiffness increase on native and glycated collagen.

4.5 Conclusions

In this chapter, I explored how glycated collagen affected PAEC CTF and stiffness in response to PA substrates of different stiffness. Although the results are only preliminary, I did show lower CTF in cells on glycated collagen compared to native collagen. Unfortunately cell stiffness did not similarly vary. More experiments need to be done to confirm these data to better understand endothelial cell mechanotransduction in a diabetic diseased environment.

5 Conclusions and Future Work

This thesis confirmed the hypothesis that collagen glycation alters endothelial cell response to substrate stiffness. Polyacrylamide substrates of different stiffness were fabricated, and native and glycated collagen were conjugated to the surfaces. Cells seeded on PA gels of different stiffness increased spread area as stiffness varied from the most compliant (0.3 kPa) to infinitely stiff (glass) on both native and glycated collagen. However, cells on glycated collagen spread significantly less compared to cells on native collagen. Cells on native collagen also showed more focal adhesions compared to cells on glycated collagen. From preliminary studies, average cell traction stress appeared lower for a cell on glycated collagen compared to a cell on native collagen on a 5 kPa gel.

This thesis shows how cellular mechanotransduction of substrate stiffness is altered in disease conditions, as cells are unable to properly spread, form focal adhesions and exert traction forces on glycated collagen coated substrates compared to cells on native

collagen. These findings shed new light on how endothelial cells may respond to collagen glycation, which leads to both ECM stiffening and altered integrin interaction.

5.1 Future Work

Cell adhesion to ECM via integrins plays an important role in endothelial cell response to substrate stiffness. Endothelial cells bind to native collagen using $\alpha_1\beta_1$ and $\alpha_2\beta_1$ integrins, but cells could bind to glycated collagen using alternative integrins other than $\alpha_2\beta_1$. Thus it is important to examine how substrate stiffness is mechanotransduced by different integrins. This could be achieved by comparing cell response to PA gels of increasing stiffness that are coated with a variety of matrix proteins, including collagen, fibronectin, vitronectin, and laminin.

The cell traction forces and stiffness experiments need to be repeated, since the cell response to PA substrates of different stiffness was not clear. Additional samples should be carefully prepared, and multiple cells should be measured for traction force microscopy. Additionally, some additional modification of the analysis method is likely needed. For AFM, additional cells need to be analyzed as well. The results presented in this thesis were only preliminary, thus further experiments are needed to fully establish the relationship between these two important cell mechanical parameters especially under glycated conditions.

Another important topic to be explored is cell migration on native and glycated collagen coated PA substrates with a rigidity gradient. Previous studies showed that fibroblasts migrate in the direction of increasing stiffness with increased migration speed and traction forces once the cells reached the rigid substrate side. Experiments on endothelial

cell migration on a PA substrate with a rigidity gradient coated with native and glycated collagen could be used to determine if cells still migrate towards the stiffer surface in a disease condition.

List of References

1. Tse, J.R., and Engler, A.J. (2010). Preparation of hydrogel substrates with tunable mechanical properties. Current protocols in cell biology / editorial board, Juan S.Bonifacino ...[et al.] *Chapter 10*, Unt10.16.

2. Plant, A.L., Bhadriraju, K., Spurlin, T.A., and Elliott, J.T. (2009). Cell response to matrix mechanics: Focus on collagen. Biochimica Et Biophysica Acta-Molecular Cell Research *1793*, 893-902.

3. Satcher Jr, R.L., and Dewey Jr, C.F. (1996). Theoretical estimates of mechanical properties of the endothelial cell cytoskeleton. Biophysical journal *71*, 109-118.

4. Janmey, P.A., and McCulloch, C.A. (2007). Cell mechanics: Integrating cell responses to mechanical stimuli. ANNUAL REVIEW OF BIOMEDICAL ENGINEERING *9*, 1-34.

5. Yeung, T., Georges, P.C., Flanagan, L.A., Marg, B., Ortiz, M., Funaki, M., Zahir, N., Ming, W.Y., Weaver, V., and Janmey, P.A. (2005). Effects of substrate stiffness on cell morphology, cytoskeletal structure, and adhesion. Cell motility and the cytoskeleton *60*, 24-34.

6. Pelham, R.J., and Wang, Y.L. (1998). Cell locomotion and focal adhesions are regulated by substrate flexibility (vol 94, pg 13661, 1997). Proceedings of the National Academy of Sciences of the United States of America *95*, 12070-12070.

7. Califano, J.P., and Reinhart-King, C.A. (2010). Substrate Stiffness and Cell Area Predict Cellular Traction Stresses in Single Cells and Cells in Contact. Cellular and Molecular Bioengineering *3*, 68-75.

8. Peyton, S.R., and Putnam, A.J. (2005). Extracellular matrix rigidity governs smooth muscle cell motility in a biphasic fashion. Journal of cellular physiology *204*, 198-209.

9. Lo, C.M., Wang, H.B., Dembo, M., and Wang, Y.L. (2000). Cell movement is guided by the rigidity of the substrate. Biophysical journal *79*, 144-152.

10. Van Vliet, K.J., Bao, G., and Suresh, S. (2003). The biomechanics toolbox: experimental approaches for living cells and biomolecules. Acta Materialia *51*, 5881-5905.

11. Dembo, M., and Wang, Y.L. (1999). Stresses at the cell-to-substrate interface during locomotion of fibroblasts. Biophysical journal *76*, 2307-2316.

12. Wang, J.H.C., and Lin, J.-S. (2007). Cell traction force and measurement methods. Biomechanics and Modeling in Mechanobiology *6*, 361-371.

13. Chopra, A., Tabdanov, E., Patel, H., Janmey, P.A., and Kresh, J.Y. (2011). Cardiac myocyte remodeling mediated by N-cadherin-dependent mechanosensing. American Journal of Physiology-Heart and Circulatory Physiology *300*, H1252-H1266.

14. Ghosh, K., Pan, Z., Guan, E., Ge, S., Liu, Y., Nakamura, T., Ren, X.-D., Rafailovich, M., and Clark, R.A.F. (2007). Cell adaptation to a physiologically relevant ECM mimic with different viscoelastic properties. Biomaterials *28*, 671-679.

15. Solon, J., Levental, I., Sengupta, K., Georges, P.C., and Janmey, P.A. (2007). Fibroblast adaptation and stiffness matching to soft elastic substrates. Biophysical journal *93*, 4453-4461.

16. Engler, A.J., Sen, S., Sweeney, H.L., and Discher, D.E. (2006). Matrix elasticity directs stem cell lineage specification. Cell *126*, 677-689.

17. Calles-Escandon, J., and Cipolla, M. (2001). Diabetes and endothelial dysfunction: A clinical perspective. Endocrine reviews *22*, 36-52.

18. Laakso, M. (1999). Hyperglycemia and cardiovascular disease in Type 2 diabetes. Diabetes *48*, 937-942.

19. Wei, M., Gaskill, S.P., Haffner, S.M., and Stern, M.P. (1998). Effects of diabetes and level of glycemia on all-cause and cardiovascular mortality - The San Antonio Heart Study. Diabetes care *21*, 1167-1172.

20. Klein, R. (1995). Hyperglycemia and Microvascular and Macrovascular Disease in Diabetes. Diabetes care *18*, 258-268.

21. Michiels, C. (2003). Endothelial cell functions. Journal of cellular physiology *196*, 430-443.

22. De Vriese, A.S., Verbeuren, T.J., Van de Voorde, J., Lameire, N.H., and Vanhoutte, P.M. (2000). Endothelial dysfunction in diabetes. British journal of pharmacology *130*, 963-974.

23. Brownlee, M. (2005). The pathobiology of diabetic complications - A unifying mechanism. Diabetes *54*, 1615-1625.

24. Avery, N.C., and Bailey, A.J. (2006). The effects of the Maillard reaction on the physical properties and cell interactions of collagen. Pathologie Biologie *54*, 387-395.

25. Bobbink, I.W.G., deBoer, H.C., Tekelenburg, W.L.H., Banga, J.D., and deGroot, P.G. (1997). Effect of extracellular matrix glycation on endothelial cell adhesion and spreading - Involvement of vitronectin. Diabetes *46*, 87-93.

26. Figueroa, D.S., Kemeny, S.F., and Clyne, A.M. (2011). Glycated Collagen Impairs Endothelial Cell Response to Cyclic Stretch RID D-5471-2011. Cellular and Molecular Bioengineering *4*, 220-230.

27. Kemeny, S.F., Figueroa, D.S., Andrews, A.M., Barbee, K.A., and Clyne, A.M. (2011). Glycated collagen alters endothelial cell actin alignment and nitric oxide release in response to fluid shear stress. Journal of Biomechanics *44*, 1927-1935.

28. Wang, N., and Ingber, D.E. (1994). Control of Cytoskeletal Mechanics by Extracellular-Matrix, Cell-Shape, and Mechanical Tension. Biophysical journal *66*, 2181-2189.

29. Ingber, D. (1991). Integrins as mechanochemical transducers. Current opinion in cell biology *3*, 841-848.

30. Redfield, M.M., Jacobsen, S.J., Borlaug, B.A., Rodeheffer, R.J., and Kass, D.A. (2005). Age- and gender-related ventricular-vascular stiffening - A community-based study. Circulation *112*, 2254-2262.

31. Wang YX, F.R.M. (2004). Vascular stiffness: measurements, mechanisms and implications. Curr Vasc Pharmacol *2*, 379 - 384.

32. Schwartz, M.A. (2009). CELL BIOLOGY The Force Is with Us. Science *323*, 588-589.

33. Peyton, S.R., Ghajar, C.M., Khatiwala, C.B., and Putnam, A.J. (2007). The emergence of ECM mechanics and cytoskeletal tension as important regulators of cell function. Cell biochemistry and biophysics *47*, 300-320.

34. Knight, C.G., Morton, L.F., Peachey, A.R., Tuckwell, D.S., Farndale, R.W., and Barnes, M.J. (2000). The collagen-binding A-domains of integrins alpha(1)beta(1) and alpha(2)beta(1) recognize the same specific amino acid sequence, GFOGER, in native (triple-helical) collagens. Journal of Biological Chemistry *275*, 35-40.

35. Di Lullo, G.A., Sweeney, S.M., Korkko, J., Ala-Kokko, L., and San Antonio, J.D. (2002). Mapping the ligand-binding sites and disease-associated mutations on the most abundant protein in the human, type I collagen. Journal of Biological Chemistry *277*, 4223-4231.

36. Tseng, Q., Duchemin-Pelletier, E., Deshiere, A., Balland, M., Guillou, H., Filhol, O., and Thery, M. (2012). Spatial organization of the extracellular matrix regulates cell-cell junction positioning. Proceedings of the National Academy of Sciences of the United States of America *109*, 1506-1511.

37. Domke, J., and Radmacher, M. (1998). Measuring the elastic properties of thin polymer films with the atomic force microscope. Langmuir *14*, 3320-3325.

38. Rape, A.D., Guo, W.-h., and Wang, Y.-l. (2011). The regulation of traction force in relation to cell shape and focal adhesions. Biomaterials *32*, 2043-2051.